AMERICAN SOCIETY FOR MICROBIOLOGY | mBio®

RESEARCH ARTICLE

SmdA is a Novel Cell Morphology Determinant in *Staphylococcus aureus*

Ine Storaker Myrbråten,[a] Gro Anita Stamsås,[a] Helena Chan,[b,c] Danae Morales Angeles,[a] Tiril Mathiesen Knutsen,[a] Zhian Salehian,[a] Volha Shapaval,[d] Daniel Straume,[a] Morten Kjos[a]

[a]Faculty of Chemistry, Biotechnology and Food Science, Norwegian University of Life Sciences, Ås, Norway
[b]Structural Cellular Biology Unit, Okinawa Institute of Science and Technology, Okinawa, Japan
[c]The ithree institute, University of Technology Sydney, Broadway, New South Wales, Australia
[d]Faculty of Science and Technology, Norwegian University of Life Sciences, Ås, Norway

ABSTRACT Cell division and cell wall synthesis in staphylococci need to be precisely coordinated and controlled to allow the cell to multiply while maintaining its nearly spherical shape. The mechanisms ensuring correct placement of the division plane and synthesis of new cell wall have been studied intensively. However, hitherto unknown factors and proteins are likely to play key roles in this complex interplay. Here, we identified and investigated a protein with a major influence on cell morphology in *Staphylococcus aureus*. The protein, named SmdA (for staphylococcal morphology determinant A), is a membrane protein with septum-enriched localization. By CRISPRi knockdown and overexpression combined with different microscopy techniques, we demonstrated that proper levels of SmdA were necessary for cell division, including septum formation and cell splitting. We also identified conserved residues in SmdA that were critical for its functionality. Pulldown and bacterial two-hybrid interaction experiments showed that SmdA interacted with several known cell division and cell wall synthesis proteins, including penicillin-binding proteins (PBPs) and EzrA. Notably, SmdA also affected susceptibility to cell wall targeting antibiotics, particularly in methicillin-resistant *S. aureus* (MRSA). Together, our results showed that *S. aureus* was dependent on balanced amounts of membrane attached SmdA to carry out proper cell division.

IMPORTANCE *Staphylococcus aureus* is an important human and animal pathogen. Antibiotic resistance is a major problem in the treatment of staphylococcal infections, and cell division and cell wall synthesis factors have previously been shown to modulate susceptibility to antibiotics in this species. Here, we investigated the function of a protein named SmdA, which was identified based on its septal localization and knockdown phenotype resulting in defective cellular morphologies. We demonstrated that this protein was critical for normal cell division in *S. aureus*. Depletion of SmdA sensitized resistant staphylococci to β-lactam antibiotics. This work revealed a new staphylococcal cell division factor and a potential future target for narrow-spectrum antimicrobials or compounds to resensitize antibiotic-resistant staphylococcal strains.

KEYWORDS cell biology, cell division, cell wall, subcellular localization

Most bacteria are surrounded by a shape-determining cell envelope that protects against lysis and interacts with the extracellular milieu. The cell envelope of the opportunistic, Gram-positive pathogen *Staphylococcus aureus* consists of a thick layer of peptidoglycan (PG) along with teichoic acids (TA) and cell wall-associated surface proteins. During a bacterial cell cycle, the synthesis of PG and TA needs to be precisely regulated and coordinated with cell division, DNA replication, and chromosome

Invited Editor Simon J. Foster, University of Sheffield

Editor Nathalie Pujol, Centre d'Immunologie de Marseille-Luminy (CIML)

Address correspondence to Morten Kjos, morten.kjos@nmbu.no.

The authors declare no conflict of interest.

Received 16 November 2021
Accepted 8 March 2022
Published 31 March 2022

segregation. Tight control of these processes is critical for staphylococcal cells to maintain their integrity and nearly spherical shape as they multiply. Therefore, they are attractive targets for antimicrobials (1). Exactly how such control is mediated in *S. aureus* is still not fully established, and hitherto unknown factors may be involved. Here, we described a new staphylococcal cell morphology determinant.

Staphylococcal cell division is initiated by the assembly of the Z-ring, consisting of polymerized FtsZ-proteins, that localizes to the future division septa (2). The Z-ring functions as a scaffold for cell division and cell wall synthesis proteins which together constitute the divisome (3). Cell division in *S. aureus* occurs in alternating orthogonal planes, meaning that the new cell division plane is always perpendicular to the previous (4). Timely and spatial control of localization of the Z-ring assembly is most likely linked with chromosome segregation and DNA replication, involving proteins such as the nucleoid occlusion factor Noc, which ensures that the cells do not establish new septa across the chromosomes (5), and CcrZ, which connects initiation of DNA replication to cell division (6). The chromosomes and chromosome segregation also contribute to establishing a physical barrier allowing the Z-ring only to be formed at an angle perpendicular to the previous division plane (4).

The Z-ring directs the synthesis of new PG in *S. aureus* to the septum. Synthesis of PG starts in the cytoplasm, where UDP-MurNAc-pentapeptide is first synthesized and then attached to the membrane by the enzyme MraY to form the PG precursor lipid I (7, 8). A GlcNAc residue and a pentaglycine side chain are attached to produce lipid II-Gly_5 (9), which is flipped to the outer leaflet of the membrane by MurJ (10, 11) where it is incorporated into the existing PG mesh by transpeptidation (TP) and transglycosylation (TG) reactions. Specifically, the shape, elongation, division, and sporulation (SEDS) proteins, FtsW and RodA with TG activity, work in pairs with monofunctional transpeptidases, the penicillin-binding proteins PBP1 and PBP3, respectively (12, 13). While the PBP1-FtsW pair is essential and performs the septal cross wall synthesis, the nonessential PBP3-RodA pair is responsible for the slight elongation taking place in *S. aureus*. Additionally, *S. aureus* possesses two other PBPs: the bifunctional PBP2 with both TG and TP activity, whose role is essential in *S. aureus*, and the low-molecular-weight PBP4, which controls the degree of PG cross-links (14–16). Finally, MRSA strains have an additional PBP, PBP2A, a transpeptidase with low-affinity for β-lactam antibiotics (17, 18). In the final step of division, PG hydrolases break covalent bonds in PG for cell wall remodeling and daughter cell splitting. The major, bifunctional autolysin Atl, together with Sle1, for which expression is regulated by the two-component system WalKR, are the primary enzymes responsible for hydrolyzing the septal PG to allow splitting of daughter cells (19–22). The actual cross wall splitting is a mechanical process occurring within milliseconds (23, 24).

The spatiotemporal control of cell division and PG synthesis is directly and indirectly influenced by several factors. One of these is the anionic TA polymers, the second major component of the cell wall, which are either covalently linked to the PG (wall teichoic acids [WTA]) or linked via a lipid-anchor to the plasma membrane (lipoteichoic acids [LTA]). Mutations in enzymes involved in either WTA or LTA biosynthesis result in cells of abnormal shape and lack of septum synthesis control, probably via different mechanisms (15, 25, 26). Furthermore, proteases, chaperones, and secretion proteins, involved in the production, folding, and/or secretion of cell cycle proteins, may also directly or indirectly affect the coordination of cell division and septum formation in *S. aureus*. For example, Clp-protease complexes can target both FtsZ and Sle1, and thereby have major effects on these processes (27–29).

Cell shape maintenance and control of cell division and septum formation are a complex interplay between many cellular processes where unknown key factors are yet to be discovered. Here, we identified a novel protein named SmdA (staphylococcal morphology determinant A). We showed that the level of the membrane attached SmdA protein was critical for maintaining normal division progression and morphology in *S. aureus* because silencing or overexpression of *smdA* resulted in defective cell

division and septal cross wall synthesis as well as increased sensitivity toward cell wall targeting antibiotics.

RESULTS

SmdA is a conserved staphylococcal membrane protein. To identify novel proteins potentially involved in cell cycle and morphology control in *S. aureus*, we performed a combined depletion and subcellular localization analysis of essential staphylococcal proteins with no annotated functions (30–32). From this, we identified a septum-enriched protein (SAOUHSC_01908, named SmdA), whose knockdown resulted in cells of variable sizes that formed large clusters (see below). The function of SmdA in *S. aureus* was investigated further here.

SmdA is a protein of 302 amino acids which is fully conserved in species within the *Staphylococcaceae* family (Fig. S1). The *smdA* gene is monocistronic and located >100 bp away from the neighboring genes (SAOUHSC_01907; unknown function, and *metK*; S-adenosylmethionine synthase). The protein had a predicted N-terminal transmembrane helix and a C-terminal cytoplasmic part with partial homology to a so-called nuclease-related domain (NERD) (PF08375, E = 1.08×10^{-5}) (Fig. 1A). The domain was named based on distant similarities to endonucleases and was found in bacterial, archaeal, and plant proteins (33). However, the functional role of NERD in bacteria has to our knowledge never been studied. SmdA is essential in transposon mutagenesis studies in *S. aureus* (30, 32). Growth analysis of SmdA CRISPRi knockdown (SmdA^{down}) in *S. aureus* SH1000 in a rich medium at 37°C resulted in a reduction in growth compared to the control strain when spotted on agar plates (Fig. 1B). The growth rate in the liquid medium was only slightly affected when CFU and the optical density at 600 nm (OD_{600}) were determined at different time points in the same culture during growth (Fig. S2A). By RT-PCR we verified that the expression of *smdA* was fully knocked down by the CRISPRi system in *S. aureus* SH1000 (Fig. S2B). Because the SmdA^{down} strains were still viable, we attempted to construct deletion mutants of *smdA* by allelic replacement with a spectinomycin resistance cassette using the pMAD-vector (34). However, we were not able to obtain the deletion mutant in *S. aureus* SH1000. Similarly, for *S. aureus* strains NCTC8325-4, HG001, and the MRSA strain COL, SmdA^{down} resulted in reduced growth on agar plates, with HG001 being most affected (Fig. 1B), but we were not able to obtain any deletion mutants in these strains. We, therefore, used the CRISPRi system in the different *S. aureus* strains to study the phenotypes of SmdA further.

Depletion and overexpression of SmdA result in cells with highly aberrant cell shapes. During the initial analysis, we observed that SmdA^{down} in *S. aureus* SH1000 resulted in clusters containing cells of variable sizes. The knockdown experiment was repeated, and exponentially growing cells were stained with fluorescent vancomycin (VanFL, binds to noncross-linked stem peptides throughout the cell wall). SmdA^{down} indeed resulted in severe phenotypic defects (Fig. 1C): increased cell clustering and a large fraction of cells with multiple septa (20.1% for SmdA^{down} as opposed to 1.6% for the control strain; Fig. 1D) and abnormal, nonspherical morphology (Fig. 1E). The SmdA^{down} cells were also significantly larger than the control strain (Fig. 1F).

Transmission and scanning electron microscopy (TEM and SEM) were used to obtain more detailed images of the defects in morphology and septal placement found in SmdA^{down} cells. Strikingly, SmdA depleted *S. aureus* SH1000 displayed highly aberrant septum formation (Fig. 2A). In addition to lysis, cells with several nonperpendicular or parallel septa were frequently observed, resulting in cells, or small cell clusters, with aberrant morphologies (Fig. 2A). This was also evident from the SEM micrographs, which showed clustered cells with various morphologies (Fig. 2B). Similar phenotypes from TEM and SEM analyses were observed for the NCTC8325-4, HG001, and COL strains, with the HG001 strain being more affected by SmdA^{down} than the other two (Fig. S3 and S4).

Because reduced levels of SmdA led to defects in cell division and morphology of *S. aureus*, we next wondered whether overexpression of SmdA would affect the cells. An ectopic copy of *smdA* under the control of an IPTG-inducible promoter in the plasmid

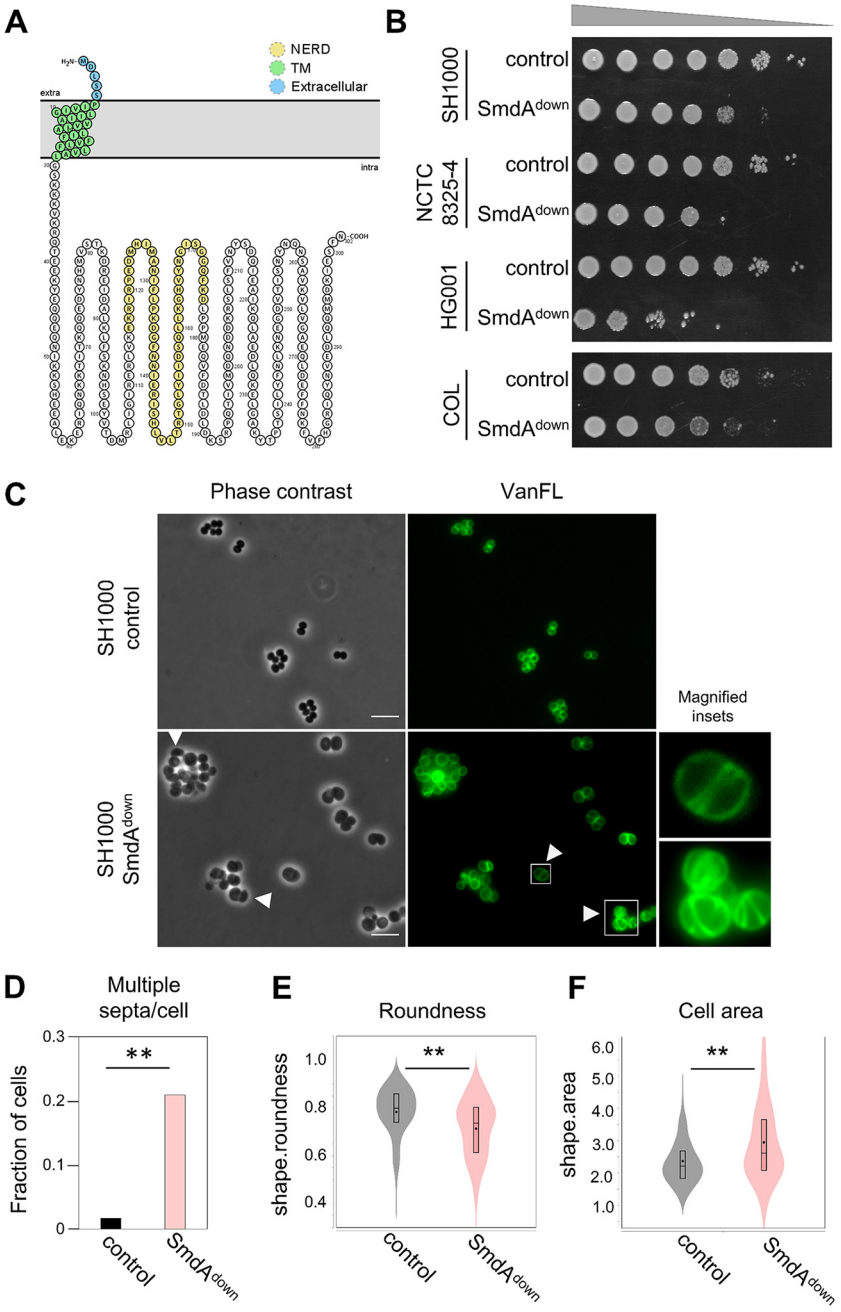

FIG 1 Phenotypes resulting from depletion of SmdA. (A) Predicted topology of SmdA using Protter (77). SmdA is predicted to have one transmembrane (TM) helix with a short extracellular N terminus and a large intracellular domain. The sequence with predicted similarity to the NERD domain is highlighted in yellow. (B) Growth on a solid medium of SmdA knockdown strains (SmdA^{down}) in *S. aureus* SH1000 (IM269), NCTC8325-4 (IM311), HG001 (IM312), and COL (IM294). Strains carrying a nontargeting sgRNA were used as controls (IM284, IM307, IM313, and IM295 for the respective strains). From noninduced overnight cultures, 10-fold dilution series were made and spotted onto plates with 300 μM isopropyl-β-D-thiogalactopyranoside (IPTG). (C) SmdA^{down} (IM269) and control strain (IM284) were analyzed by phase-contrast and fluorescence microscopy of cells stained with the cell wall label VanFL. White arrows point at misshaped cells and cells with perturbed septum formation. Magnified insets of representative cells are shown for the VanFL micrographs. Scale bars, 5 μm. (D) Fraction of cells with multiple septa per cell for the SmdA^{down} strain IM269 (n = 225) and the nontarget control strain IM284 (n = 242) are plotted. The asterisks indicate a significant difference (Fisher's exact test, $P < 0.001$). (E) Cell roundness, as determined using MicrobeJ, was used as a measure of the morphology of the cells. Spherical cells will have values close to 1. Cell roundness measures for the control strain IM284 (n = 198) and the SmdA^{down} strain IM269 (n = 191) are plotted. (F) Cell area (in μm^2) as determined using MicrobeJ of the control strain IM284 (n = 198) and the SmdA^{down} strain IM269 (n = 191). (E and F) Significant differences between the distributions are indicated by asterisks (**, $P < 0.001$). P values were derived from a Mann-Whitney test.

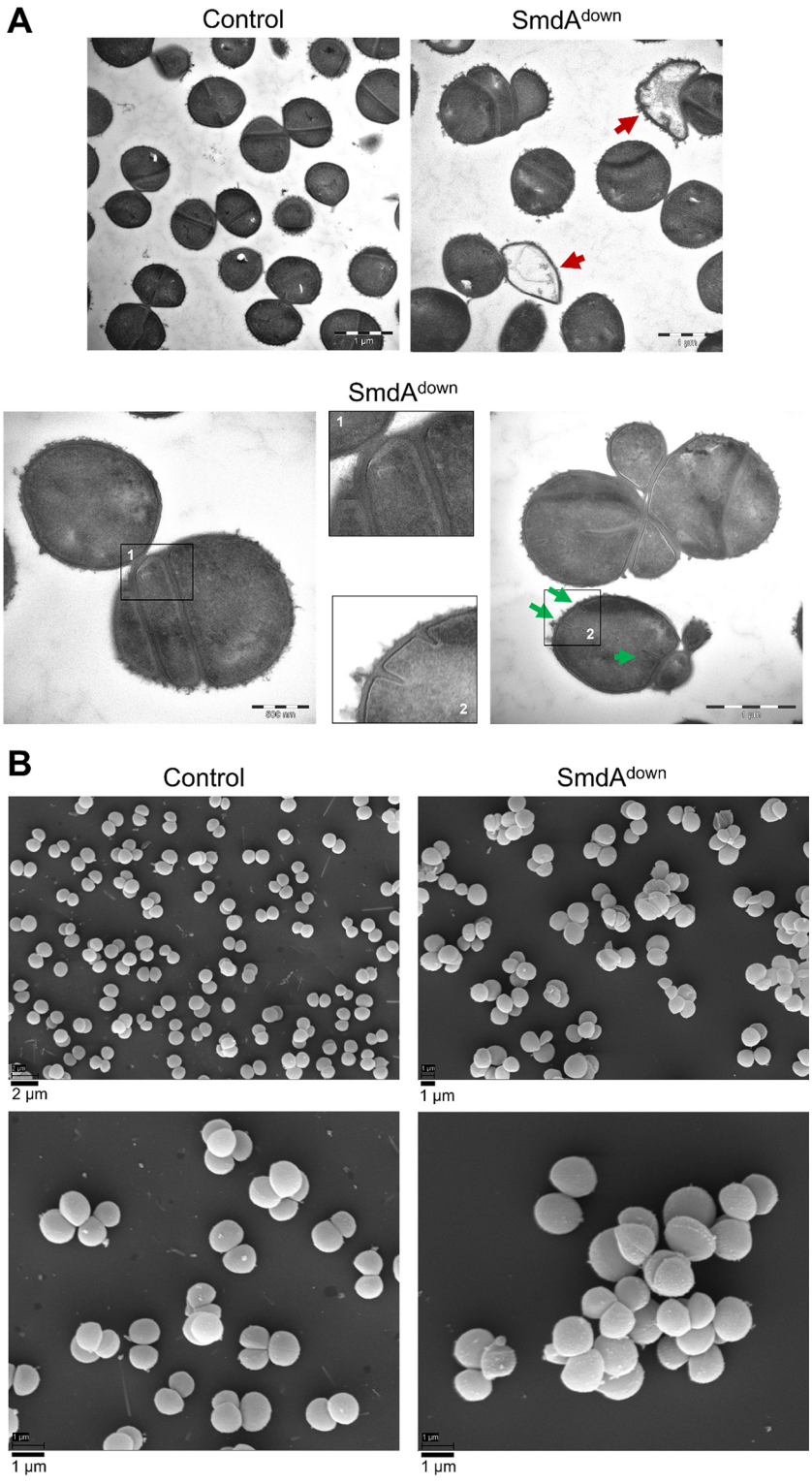

FIG 2 SmdA^{down} in *S. aureus* SH1000 visualized by electron microscopy. (A) Transmission electron and (B) scanning electron micrographs of SH1000 CRISPRi control strain (IM284) and SH1000 SmdA^{down} (IM269). In (A), red arrows in the TEM micrographs point at lysed cells. Representative examples of cells with parallel septa or multiple septa are shown. Green arrows point to the initiation of septum synthesis at multiple sites within the same cell. Different magnifications are shown, indicated by the scale bars.

TABLE 1 MIC (MIC, in μg/mL) of different antimicrobials when SmdA was depleted in *S. aureus* SH1000 and COL

	S. aureus SH1000 (MSSA)			*S. aureus* COL (MRSA)		
Antibiotics	**SmdA^{down}**	**Control**	**Fold change**	**SmdA^{down}**	**Control**	**Fold change**
Oxacillin	0.12	0.24	2	64–128	256	2–4
Cefotaxime	2	2	1	50	400	8
Cefoxitin	1	2	2	47–94	188	2–4
Imipenem	0.016	0.016	1	150	>300	>2
Vancomycin	2.5	2.5	1	2.5	2.5	1
Tetracycline	0.05	0.1–0.2	2–4	≥64	≥64	1
Ciprofloxacin	0.32	0.32	1	0.32	0.32	1
Tunicamycin	0.094	6	64	24	>96	>4
Targocil	1	1	1	1	1	1
Congo Red	256	>1,024	>4	512–1,024	>1,024	≥2

pLOW (35) was expressed in *S. aureus* NCTC8325-4. For SmdA^{down}, the cells were stained with VanFL (Fig. S5A). Although less evident than for SmdA^{down}, overexpression of SmdA also resulted in clusters of cells with several septa per cell as defined by VanFL staining (Fig. S5A) (3.9%, n = 181 for SmdA overexpression, compared to 20.1% for SmdA^{down}, and 1.6% for the control). Together, these knockdown and overexpression experiments demonstrate that septum formation and splitting in *S. aureus* were dependent on proper levels of SmdA.

Depletion of SmdA results in increased sensitivity toward antimicrobials targeting cell wall synthesis. Given the negative effect SmdA depletion had on cell morphology and division, we reasoned that reduced expression of SmdA could influence the sensitivity of *S. aureus* to cell wall targeting antibiotics. To test this, SmdA^{down} strains were treated with PBP-targeting β-lactams (oxacillin, cefotaxime, cefoxitin, and imipenem), the glycopeptide vancomycin (blocking cell wall synthesis by targeting the terminal D-Ala-D-Ala on the stem peptides of nascent PG (36)), tunicamycin (targeting TarO and MraY, enzymes involved in the early stages of WTA and PG synthesis, respectively (37)), targocil (targeting the WTA exporter TarG (38)) and Congo red (inhibitor of the LTA biosynthesis enzyme LtaS (39)) (Table 1). Two antibiotics with alternative targets, tetracycline (targeting protein synthesis) and ciprofloxacin (a quinolone targeting DNA synthesis), were also included.

For the methicillin-susceptible *S. aureus* (MSSA) strain SH1000, a 2-fold reduction in MIC, compared to the control, was observed for oxacillin and cefoxitin in SmdA^{down}. More notably, in the MRSA strain COL, SmdA^{down} sensitized the COL strain toward all β-lactams with a 2 to 8-fold reduction in MIC compared to the control (Table 1). SmdA depletion did not seem to significantly influence vancomycin susceptibility. Strikingly, however, we observed that SmdA^{down} cells became highly sensitive toward tunicamycin, with a 64-fold reduction in MIC compared to the control for *S. aureus* SH1000 and >4-fold reduction for COL (40, 41). We therefore also tested the tunicamycin sensitivity of the NCTC8325-4 and HG001 SmdA^{down} strains, which also showed increased susceptibility toward tunicamycin (HG001; 125-fold reduced MIC and NCTC8325-4; 4-fold reduced). While no difference in MIC was observed for targocil, the SmdA^{down} strains also displayed increased sensitivity toward Congo red. Finally, SmdA depletion in *S. aureus* SH1000 led to a 2 to 4-fold reduction in MIC against tetracycline compared to the control. However, depletion of SmdA in COL did not change its sensitivity toward tetracycline or ciprofloxacin (Table 1).

SmdA has no major effects on the TA biosynthetic pathways. The increased sensitivity to tunicamycin and Congo red in SmdA^{down} strains, prompted us to study whether there were any major alterations in the TA in these cells, although it was also noted that no changes in sensitivity were observed for the WTA export inhibitor targocil (Table 1). Notably, the SmdA^{down} strain displayed morphologies reminiscent of what has previously been reported for cells depleted of TA, i.e., with larger cell sizes, cells with irregular septum formations, and reduced splitting (26, 37, 38, 42). It has

previously been shown that there was a synthetic lethal relationship between the WTA and LTA biosynthetic pathways (42, 43), and it could therefore be hypothesized that hypersensitivity to tunicamycin could result from deficient LTA biosynthesis in the *smdA*^{down} mutants, Using an anti-LTA antibody, we compared the quantity and lengths of LTA in the SmdA^{down} and control strains for SH1000, NCTC8325-4, HG001 and COL (Fig. S6A). For HG001, the strain with the most severe division defects, we observed a reduction in LTA amounts in SmdA^{down} and this can contribute to the severe phenotype of this strain. However, no consistent changes in LTA amounts or lengths were observed between the SmdA depletions and the controls in the four strains. Furthermore, we could not detect any LTA release into the growth medium in the depletion strains, indicating that the stability of LTA (44) was intact (Fig. S6B). We, therefore, conclude that SmdA does not have any consistent effect on LTA synthesis across strains.

WTA has been shown to protect cells from the LTA-inhibitor Congo red. Without WTA, cells became hypersensitive toward Congo red (MIC of <4 μg/mL for *tarO* deletion mutants and >1024 μg/mL for wild-type cells) (45). Although to a much lesser degree, SmdA depletion strains were also more sensitive to Congo red compared to the controls (Table 1). We, therefore, investigated whether WTA could be disturbed in a SmdA^{down} strain. Cells without WTA have previously been shown to lack the dark, electron-dense layer observed in TEM images of crosswalls of *S. aureus* wild-type cells (Fig. S6C) (37, 46). TEM images of TarO^{down} and SmdA^{down} showed that TarO^{down}, as expected (37, 46), lacked this dark, high-density layer, while it was still present in the SmdA^{down} strain, suggesting that WTA was still produced (Fig. S6C). We also performed Fourier transform infrared spectroscopy (FTIR), which has been used before to detect differences in the composition of WTA due to variable glycosylation patterns (44, 47). As expected, changes in the FTIR spectra were evident in the polysaccharide region (1200 cm^{-1} to 800 cm^{-1}) for the TarO^{down} strain compared to the control, with the most significant differences recorded for the peaks at 1076 cm^{-1}, 1048 cm^{-1}, 1033 cm^{-1}, and 1000 to 970 cm^{-1}, representing α- and β-glycosidic bonds in WTA (47). However, no changes were observed between SmdA^{down} and the control (Fig. S6D). Together, these results suggested that SmdA has no major effect on the WTA biosynthetic pathway.

SmdA is important in several stages of staphylococcal cell division. To identify potential protein interaction partners of SmdA, we next performed a protein pulldown experiment using GFP-trapping with a chromosomal *smdA-m*(*sf*)*gfp* fusion strain. Interestingly, the major staphylococcal autolysin Atl, as well as the bifunctional PBP2, were identified along with 12 other proteins (Table S1). The experiment was repeated in a strain with a plasmid-based expression of SmdA-m(sf)GFP, and this setup resulted in an extended list of proteins that were pulled down, probably due to the elevated expression of SmdA-m(sf)GFP. Selecting the proteins for which at least 10 unique peptides were detected and with a fold change of >2 compared to the control, resulting in a list of 57 proteins (Table S1). Several proteins with activity involved in protein folding, secretion, and/or degradation (e.g., FtsH, PrsA, SpsB, ClpB, ClpC, SecD) were identified in this assay, in addition to the penicillin-binding proteins PBP1, PBP2, PBP3, and the early division protein EzrA. All the 14 proteins identified in the initial experiment were also pulled down in the second experiment.

Bacterial two-hybrid analyses of the SmdA-PBP1-3 and SmdA-EzrA were performed to see whether these interactions could be reproduced in a heterologous system. The proteins were fused either N- or C-terminally to the domains of adenylate cyclase, an enzyme that catalyzes the production of cyclic AMP (cAMP) and eventually induction of β-galactosidase production when brought in proximity by the interaction between the target proteins. Indeed, SmdA interacted with PBP2, as well as PBP1, PBP3, and EzrA in the two-hybrid assays (Fig. 3A). By expressing a version of SmdA without its N-terminal membrane domain (SmdAΔTMH), we also showed that the observed interactions between SmdA and the PBPs in this assay occurred via the transmembrane segment, while the interaction with EzrA was retained for SmdAΔTMH. The latter suggests

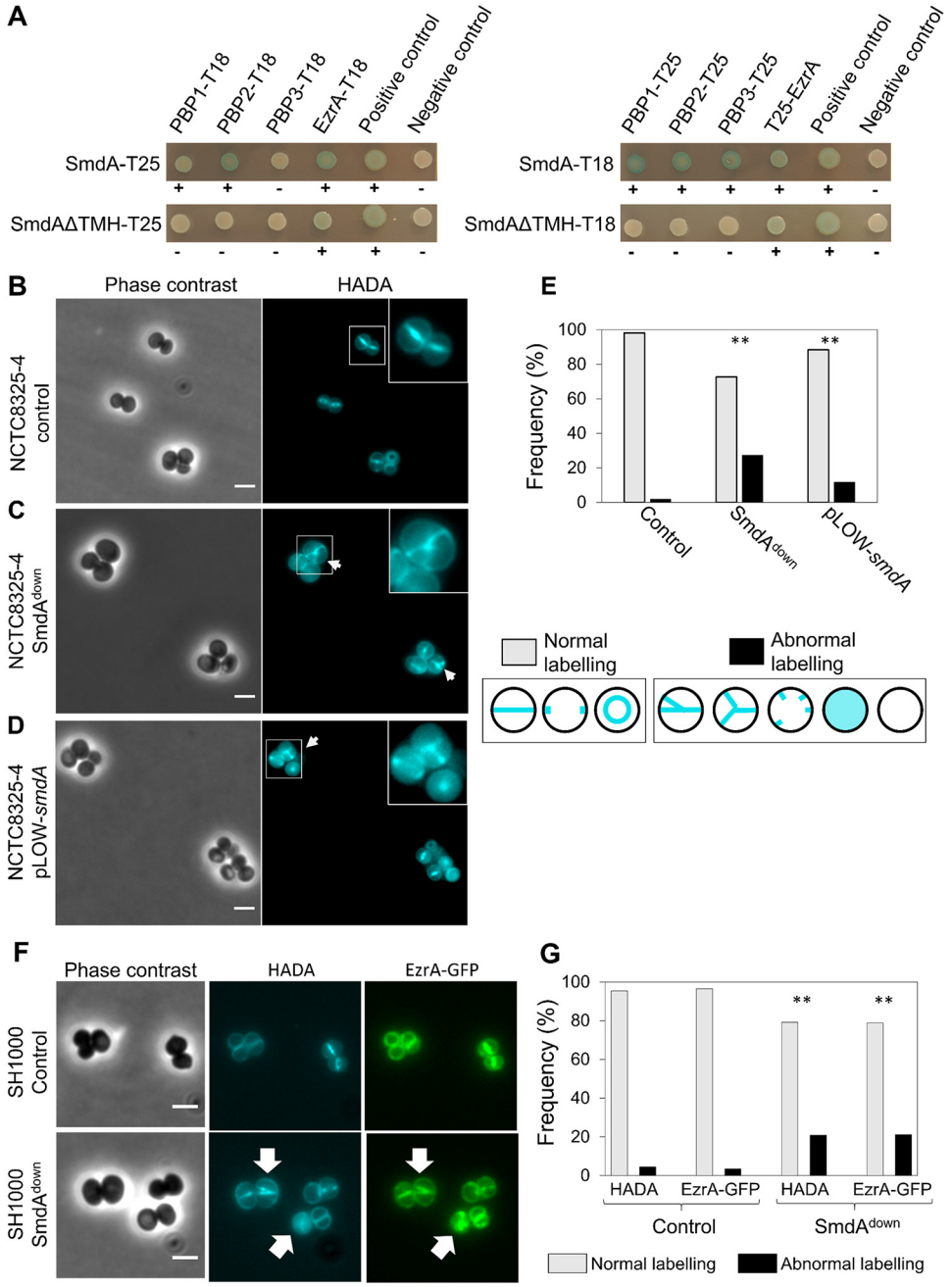

FIG 3 SmdA interacts with important cell division proteins and is necessary for proper localization of EzrA and peptidoglycan synthesis. (A) Protein-protein interactions were tested with bacterial two-hybrid assays, where SmdA and SmdAΔTMH were tested against PBP1, PBP2, PBP3, and EzrA. The proteins were fused to the T18 or T25 domains as indicated. Blue bacterial spots and plus signs indicate positive interactions and white spots and minus symbols indicate no interaction. (B to D) Micrographs of HADA labeled *S. aureus* NCTC8325-4 with depletion and overexpression of SmdA. Arrows point at cells with misplaced septum synthesis. Scale bars, 2 μm. (B) CRISPRi control strain, IM307 (C) SmdA^{down} strain, IM311 and (D) SmdA overexpression strain, MK1866. (E) Frequency plot of cells with normal or abnormal HADA labeling pattern. Categorization of normal or abnormal labeling patterns is indicated. The number of cells analyzed was 259, 179, and 189 for (B to D), respectively. The asterisks indicate a significant difference from the control (Fisher's exact test, $P < 0.001$). (F) Micrographs showing colocalization of EzrA-GFP and HADA incorporation in *S. aureus* SH1000 strains with (MK1952) or without (MK1953) knockdown of SmdA. Phase-contrast and fluorescence images of HADA labeling and GFP (EzrA-GFP) are shown. Scale bars, 2 μm. Arrows point to cells with abnormal localization of both HADA and EzrA-GFP. (G) Frequencies of cells (from [F]) with normal or abnormal localization of HADA and EzrA-GFP are plotted. The number of cells analyzed was 285 (for MK1953) and 298 (for MK1952). The asterisks indicate significant differences from the respective controls (Fisher's exact test, $P < 0.001$).

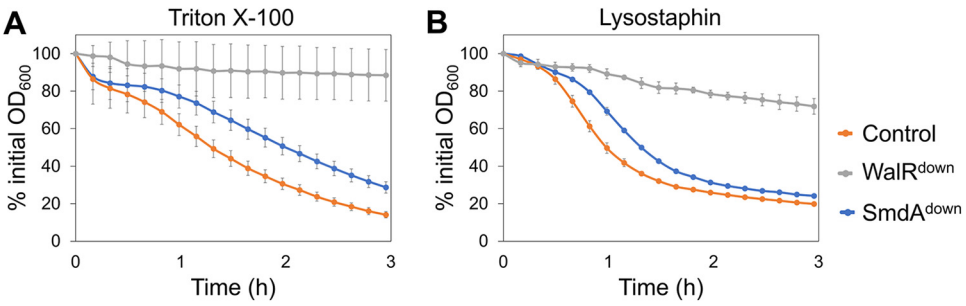

FIG 4 Autolysis of *S. aureus* SH1000 depletion strains (control = IM284; WalR^{down} = IM293; SmdA^{down} = IM269) measured in the presence of (A) 0.5% Triton X-100 and (B) 100 ng/mL lysostaphin. Results presented as % of initial OD_{600}. Error bars represent standard error calculated from four technical replicates.

that EzrA interacted with the intracellular part of SmdA (Fig. 1A). Furthermore, we also showed that SmdA could self-interact, and this interaction was dependent on the transmembrane helix (Fig. S7).

The observed interactions between SmdA and PBPs may suggest that SmdA is somehow important for proper regulation and/or localization of PBPs in *S. aureus* (Fig. 1 and 2). The VanFL approach used above (Fig. 1C) labeled non-crosslinked PG throughout the cell surface. Therefore, to determine more precisely the sites of active PG synthesis in *S. aureus* NCTC8325-4 SmdA^{down} and SmdA overexpression cells, we pulse-labeled the cells for 90 sec with the fluorescent D-amino acid 7-hydroxycoumarin carbonyl amino-D-alanine (HADA), a molecule that is integrated into PG by the specific activity of transpeptidases (48). In the control cells, the expected midcell-localized band was observed (Fig. 3B). However, in the SmdA^{down} strain, we observed a more diffuse HADA signal with PG synthesis often occurring at several sites within the cell, forming patterns visible as crosses or Y-shapes (Fig. 3C). Similar observations were made in the cells overexpressing SmdA, although with a lower frequency (Fig. 3D and E). Thus, the site of active transpeptidation, and likely at least one of the PBPs, were mislocalized when the levels of SmdA were altered.

Moreover, we also studied whether SmdA could affect the localization of EzrA by knocking down *smdA* in a strain expressing a chromosomal *ezrA-gfp* fusion (Fig. 3F). Indeed, abnormal localization patterns for EzrA-GFP were observed with similar frequency as the abnormal HADA labeling (Fig. 3G). These results suggest that depletion of SmdA, directly or indirectly, influenced the localization of both early and late divisome proteins in *S. aureus*.

Furthermore, the major autolysin Atl was also pulled down with SmdA. Atl is a secreted multidomain enzyme, which is processed to an acetylmuramyl-L-alanine amidase and β-N-acetylglucosaminidase, involved in septal cross wall splitting resulting in daughter cell separation (19). SmdA^{down} cells frequently displayed increased clustering (Fig. 2, Fig. S4). This indicated reduced cross wall splitting, a phenotype also observed in Δ*atl* mutants and WalKR depleted cells (22, 49). WalKR is the two-component regulatory system controlling the expression of *atl* and other cell wall hydrolase encoding genes (22). To assess the reduced cross wall splitting phenotype in more detail, we performed Triton X-100-induced autolysis assays on the cultures. Indeed, reduced autolysis was observed in SmdA^{down} cells, demonstrating reduced autolytic activity (Fig. 4A). The lysostaphin sensitivity was also reduced (Fig. 4B), suggesting alterations in the cell wall affecting the lytic properties of this enzyme. It should be noted that the resistance toward Triton X-100- and lysostaphin-induced autolysis in the SmdA^{down} strain was reduced compared to the control strain, where *walR* and all the regulated autolysins were knocked down. It should also be noted that Triton-X-induced autolysis was not severely altered upon overexpression of SmdA (Fig. S5B).

SmdA localizes at the septal region after FtsZ. The SmdA-m(sf)GFP fusion protein displayed a septum-enriched signal when expressed ectopically from the low copy-

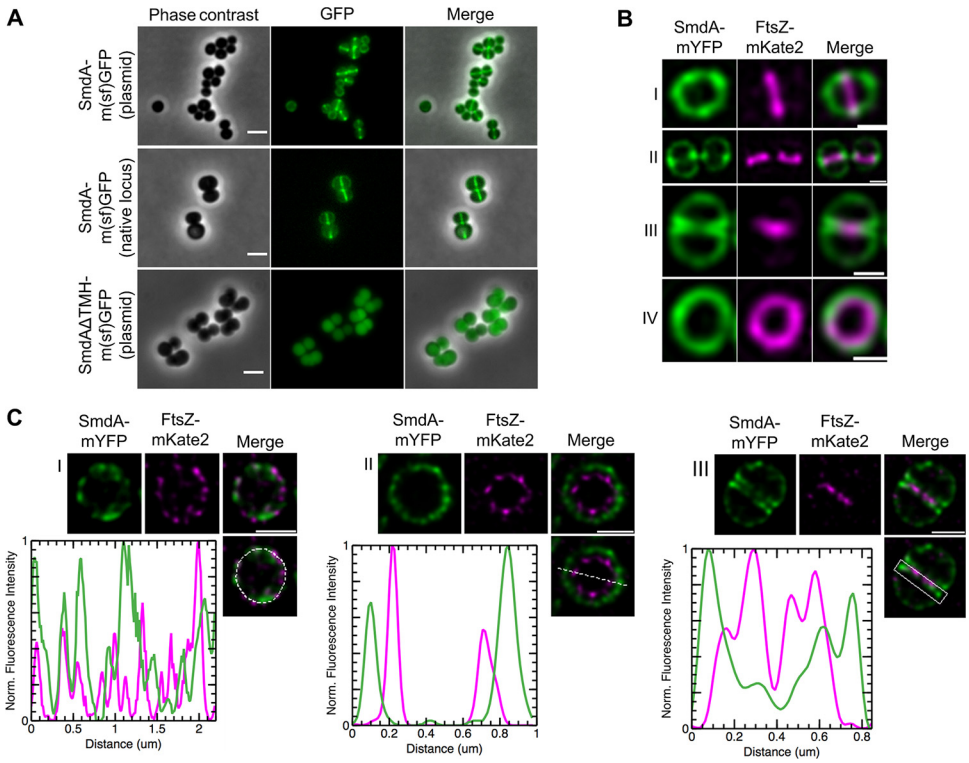

FIG 5 Subcellular localization analysis of SmdA. (A) Micrographs of cells with induced expression of SmdA-m(sf)GFP from a plasmid (top panel, IM104), native chromosomal expression of the SmdA-m(sf)GFP fusion protein (middle panel, IM308), and expression of SmdAΔTMH-m(sf)GFP from a plasmid (bottom panel, IM373). Scale bars, 2 μm. (B) SIM images of fixed *S. aureus* SH1000 with plasmid-expressed SmdA-mYFP and FtsZ-mKate2 (HC060). (B) Side-view of a cell showing that FtsZ localizes at septum before the arrival of SmdA (I). As cell division progresses, SmdA concentrates at sites where septum formation is initiated (II) and displays a septal localization at the two septal membranes as FtsZ constricts and septum formation proceeds (III). Top-view of a cell showing the FtsZ-ring inside the SmdA-ring (IV). All scale bars, 0.5 μm. (C) STED images of fixed *S. aureus* SH1000 with plasmid-expressed SmdA-mYFP and FtsZ-mKate2 (HC060), where line scans show fluorescence intensity of selected areas. (C) At an early stage of cell division, the rings of both SmdA and FtsZ had a similar diameter but do not overlap in their distribution, and a heterogeneous distribution with a patchy signal was observed (I). Top-view of a cell as cell division progresses, with the FtsZ-ring laying inside SmdA, approximately 100 to 150 nm apart from each other (II). Side-view of a cell showing how FtsZ was located innermost, and how SmdA was located at the two septal membranes (III). Scale bars, 0.5 μm.

number plasmid pLOW (Fig. 5A). To analyze the SmdA localization with native expression levels, a chromosomally integrated version of *smdA-m*(*sf*)*gfp* was made in which SmdA was expressed with m(sf)GFP fused to its C terminus. Localization analyses in these cells further confirmed the septum-enriched localization of the fusion protein (Fig. 5A) with an average septum/periphery fluorescence signal ratio of 3.4 (n = 52, see Materials and Methods). To visualize the localization of SmdA relative to the cell division process, we used FtsZ as a marker. Expression of *ftsZ*-fusion genes in the *smdA-m*(*sf*)*gfp* chromosomal fusion strain, however, only resulted in strains with extremely poor growth, suggesting that the cells did not tolerate such double-labeling. Instead, we created a double-labeled strain in which SmdA-mYFP and FtsZ-mKate2 were coexpressed from plasmids, while the native *smdA* and *ftsZ* genes were still present on the chromosome. Structured illumination microscopy (SIM) analysis showed that SmdA-mYFP was localized around in the membrane when the Z-ring was formed (Fig. 5B) and that a septum-enriched localization occurred as the septal cross wall was being synthesized. This was further confirmed by stimulated emission depletion (STED) microscopy analysis (Fig. 5C). STED imaging also revealed that there was no apparent colocalization of SmdA-mYFP and FtsZ-mKate2 in newborn cells before FtsZ-constriction initiates. Combined, the localization of SmdA was reminiscent of the localization

of PBPs in *S. aureus* (11) but appeared to localize to the septal area after the early divisome proteins such as EzrA (50, 51).

The SmdA protein was anchored to the membrane by a single transmembrane helix (Fig. 1A). To verify its significance for the septal localization, we ectopically expressed a version of SmdA without the transmembrane helix (SmdAΔTMH). The N-terminally truncated SmdAΔTMH-m(sf)GFP localized to the cytoplasm of the cells (Fig. 5A). This showed that, while the transmembrane helix is critical for protein-protein interactions and subcellular localization of SmdA, the interaction observed between EzrA and SmdAΔTMH (and full-length SmdA) (Fig. 3A) is probably not involved in determining the localization of this protein.

During these latter experiments, we noticed that SmdAΔTMH-m(sf)GFP overexpression led to cells with obvious morphology defects. Overexpression of SmdAΔTMH (without the GFP-tag) (Fig. 6A) strikingly resulted in a more extreme phenotype than overexpression of full-length SmdA (Fig. 3D, Fig. S5). The cells were often inflated or with a bean-shaped appearance (Fig. 6A). HADA pulse-labeling of these cells revealed a highly abnormal PG incorporation pattern, with the fluorescent signal forming both condensed clumps and Y-shapes in different directions in almost 50% of the cells (Fig. 6A and B). This demonstrats that membrane attachment is critical for the localization and function of SmdA.

Conserved amino acids in the predicted NERD domain were critical for the function of SmdA. The functional importance of the NERD domain (Fig. 1A) has, to our knowledge, neither been studied nor verified previously in any bacterial protein. As mentioned, we observed that overexpression of SmdAΔTMH led to severe phenotypic changes in the staphylococcal morphology (Fig. 6A). We decided to use this as a tool to gain insight into whether the predicted NERD domain was important for the function of SmdA. Multiple sequence alignment of SmdA proteins from different staphylococcal species (Fig. S1) revealed conserved residues in this domain, and site-directed mutagenesis was used to create two versions of SmdAΔTMH containing mutations in the NERD domain: one in which H145 was changed to Ala (mut1) and a second containing the mutations R150A and T151A (mut2). Furthermore, we also observed from the alignment that the C terminus of SmdA was highly conserved (Fig. S1), and another C-terminally mutated variant was created (mut3; F280A, H281A). The three-dimensional structure of SmdA, predicted by AlphaFold (52), suggested that the N-terminal part of the protein folded into a long α-helix and that the NERD domain was located within the C-terminal structured part of the protein (Fig. 6C [II]). The mutated SmdAΔTMH versions were overexpressed in a wild-type background. Expression of these mutated variants partially or fully abolished the phenotypic defects observed when overexpressing the nonmutated SmdAΔTMH version. HADA staining of mut1 (H145A) showed septum placement and PG synthesis comparable to wild-type cells, while mut2 (R150A, T151A) and mut3 (F280A, H281A) also reduced the functionality of the protein (Fig. 6A and B). Furthermore, the growth inhibition upon overexpression of SmdAΔTMH (Fig. 6D) was abolished when the mutated variants were expressed under the same conditions. This strongly suggests that the given residues in both the predicted NERD and the conserved C terminus are important for the function of SmdA.

DISCUSSION

The results presented here provide the first functional insights into the conserved staphylococcal protein SAOUHSC_01908, here named SmdA. SmdA, a protein conserved within the *Staphylococcaceae* family, is critical for maintaining cell morphology and for proper progression of cell division in different *S. aureus* strains (including MRSA and MSSA). Unbalanced levels, as well as loss of proper subcellular localization, of SmdA, resulted in severe cell morphology defects due to mislocalized cell division, uncontrolled cell wall synthesis, and lack of proper cross wall splitting.

We observed that knockdown of SmdA increased the sensitivity of *S. aureus* to several cell wall-targeting antibiotics, including β-lactams and tunicamycin (Table 1).

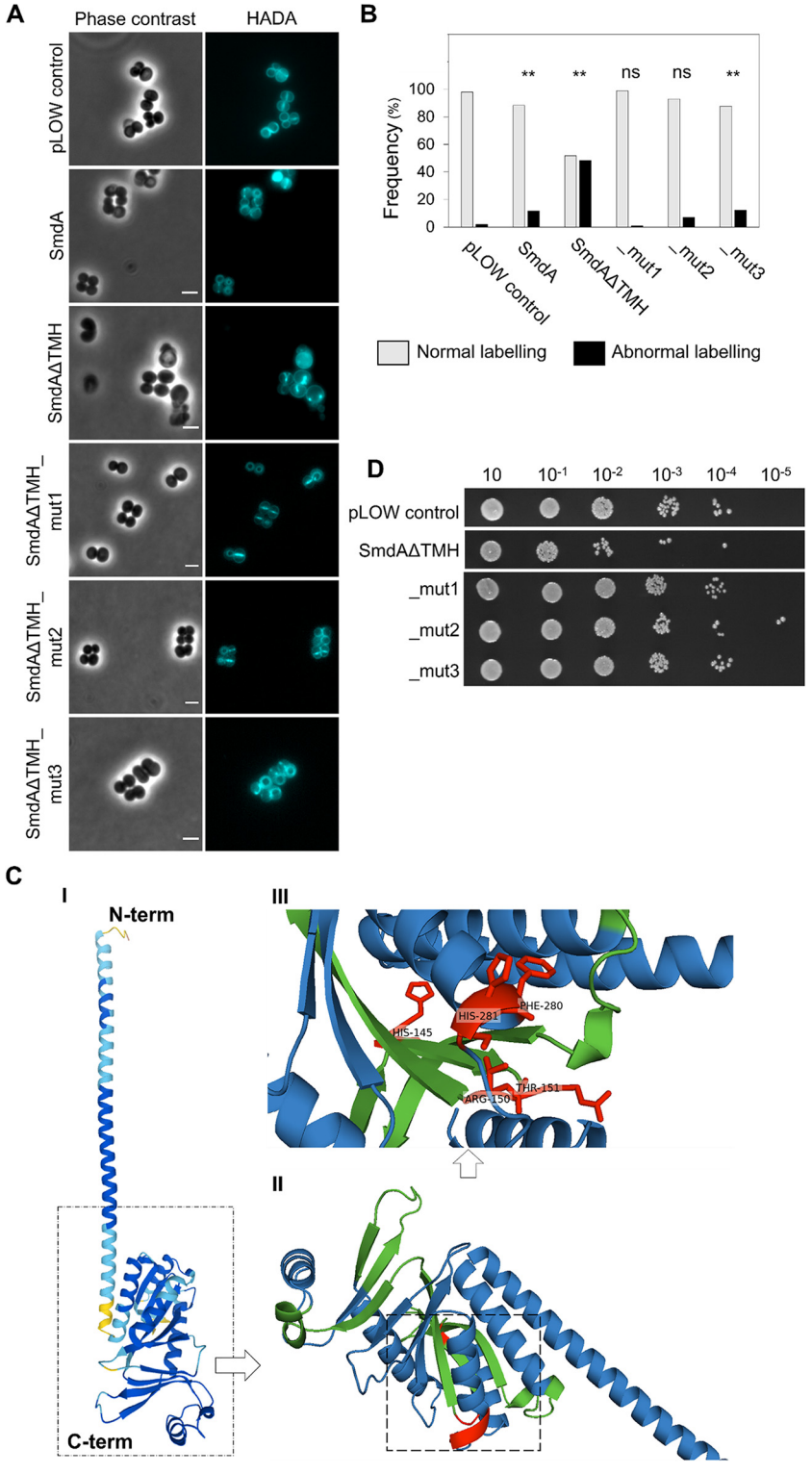

FIG 6 Membrane attachment and the NERD domain are important for SmdA function. (A) HADA stained *S. aureus* NCTC8325-4 control cells not expressing any SmdA-variant (pLOW control, IM307), cells overexpressing full-length SmdA (MK1866), and cells overexpressing SmdAΔTMH (MK1911), SmdAΔTMH_mut1 (IM377), _mut2 (IM378), and _mut3 (IM379). Scale bars, 2 μm. (B) The frequency of cells from (A) with normal or abnormal HADA staining is plotted. The number of cells plotted were 259 the pLOW control, 180 for SmdA, 82 for SmdAΔTMH, 101 for _mut1, 113 for _mut2, and 122 for _mut3. The asterisks indicate a significant difference from the pLOW control strain (Fisher's exact test, $P < 0.001$). ns indicates that there was no significant difference. (C) Structure of SmdA, predicted by AlphaFold (52), where (I) shows the structure colored by a "per-residue confidence score" (pLDDT)

(Continued on next page)

Many of the frequently used antibiotics, including β-lactams, target cell wall synthesis, but the rise of both methicillin-resistant and vancomycin-resistant *S. aureus* (MRSA and VRSA) have made *S. aureus* infections more difficult to treat and novel anti-staphylococcal targets and strategies are needed. Targeting cell cycle proteins have been shown to resensitize resistant staphylococci toward existing antibiotics due to synergistic effects (53–55). For example, the inactivation of some proteins involved in WTA synthesis sensitizes MRSA to β-lactams (37, 56). The same was also the case for a diversity of factors contributing to cell division and cell wall biogenesis, including FtsZ, FtsA, PBP4, and most proteins involved in the PG synthesis pathway (55). The secretion-associated proteins SecDF and the chaperones PrsA and HtrA1 have also been tightly linked to β-lactam sensitivity (57, 58), and recently, inactivation of the autolytic cell wall amidase Sle1 (21), or the membrane proteins AuxA and AuxB (44), was shown to result in increased sensitivity to β-lactams. Mechanisms of resensitization in these cases vary and may be a result of a weakened cell wall and inactivation or mislocalization of PG synthesis, including the key resistance determinant PBP2A. The large number of factors affecting β-lactam sensitivity reflects the tight links between different processes involved in cell wall biosynthesis, and most likely SmdA affects several steps in the cell division process (Fig. 1 and 3).

The exact mechanism by which SmdA affects these processes remains to be determined. Our results suggested that cell division and PG synthesis, but not teichoic acid biosynthesis, was affected. This is supported by observations showing mislocalization of cell division and PG synthesis in SmdA^{down} cells (Fig. 1 and 3). Furthermore, SmdA^{down} cells displayed hypersensitivity toward tunicamycin (targeting enzymes involved both in PG and WTA synthesis) but not toward targocil (targeting the WTA exporter only) (38). SmdA may influence the localization of cell division and cell wall synthesis by direct protein-protein interactions. This is supported by the SmdA-EzrA and SmdA-PBP1-3 interactions, combined with the abnormal localization of EzrA-GFP and HADA incorporation in SmdA^{down} cells (Fig. 3). The division defects observed in SmdA^{down} cells (Fig. 1 and 3) are reminiscent of previous studies of *ezrA* null mutants, strains with point mutations in FtsZ, or cells exposed to Z-ring inhibitors (50, 51, 59, 60). However, the contribution of the identified interactions to the observed phenotypes must be investigated further, particularly because the subcellular localization of SmdA-m(sf)GFP does not appear to overlap the Z-ring throughout the cell cycle. The SmdA localization, which depends on the transmembrane helix, is instead more similar to the reported localization of PBPs (Fig. 5) (11, 50, 51).

Lack of cross wall splitting is another prominent feature of the SmdA depleted cells (Fig. 2 and 4). After septum formation, cells remain attached, forming clusters of misshaped cells. Indeed, the autolytic activity was reduced in the SmdA^{down} cells (Fig. 4). The major autolysin Atl was also pulled down together with SmdA-m(sf)GFP as one of the major hits (Table S1). Atl is an extracellular processed protein whose amidase and glucosaminidase domains together process PG in the septum to allow splitting. It is possible that SmdA somehow influences the export or processing of Atl. In this context, it is interesting to note that proteases, foldases, and chaperones (FtsH, PrsA, SpsB, ClpC, ClpB, HtrA1) were also pulled down with SmdA (Table S1). It remains to be determined whether these interactions have any functional relevance. However, perturbation of such pathways may have major consequences for cell division and septal placement because they are important for the proper folding and secretion of key proteins involved in such processes. This has, for example, previously been demonstrated for the chaperone ClpX, which is critical for the coordination of autolysins and cell division pro-

FIG 6 Legend (Continued)
with dark blue pLDDT > 90, light blue 90 > pLDDT > 70, and yellow 70 > pLDDT > 50, (II) shows the structured domain magnified with the predicted NERD colored in green and residues that have been mutated in red. A magnified inset of (II) with annotated residues (III). The positions of the mutated residues are indicated in red. (D) Growth assay on a solid medium of *S. aureus* NCTC8325-4 expressing SmdAΔTMH, SmdAΔTMH_mut1, _mut2, and _mut3.

teins (29). Involvement in such a mechanism could also explain the pleiotropic phenotypes observed in SmdA^{down} cells, affecting several stages in the cell division process.

A part of SmdA displays limited similarity to the so-called nuclease-related domain (NERD). This domain, which is found in a broad range of bacterial species and some archaea and plants, was initially identified on a virulence-plasmid from *Bacillus anthracis* (33) and was later suggested to belong to a superfamily of phosphodiesterases (61). Most NERD proteins are single-domain proteins, but they are also occasionally found together with a kinase-, pseudokinase, or helicase domain (62). The actual function of the NERD, to our knowledge, has not been studied experimentally. The results here showed that conserved residues in the predicted NERD were important for the functionality of SmdA, thus demonstrating for the first time a functional role of this domain (Fig. 6). Although highly speculative at this point, it would be interesting if a cell division factor such as SmdA had DNA-interacting capabilities and thus forming a potential link between the membrane-associated cell division proteins and the nucleoid. It should also be noted that several of the most conserved residues of the NERD domain (33) are not found in SmdA, suggesting a functional diversity among proteins harboring homology to this domain and implying that the NERD of SmdA may have functions unrelated to the nucleoid.

It is also interesting to note that the effect of SmdA knockdown was different between strains. For example, SmdA^{down} resulted in a more severe phenotype in HG001 compared to NCTC8325-4 and SH1000 (Fig. 1, Fig. S3 and S4), although these strains derive from the same parent (63). While HG001 contains prophages, NCTC8325-4 and SH1000 have been cured of these, and it could, for example, be speculated that the stress imposed by knockdown of SmdA somehow results in prophage induction in HG001 and a more severe phenotype. Understanding these and other strain differences could also help to further pinpoint the exact function of SmdA.

The staphylococcal genome encodes hundreds of essential proteins, which all represent potential target sites for antimicrobials. To be able to fully exploit the antibiotic target repertoire, it is critical to understand how essential proteins are involved and linked between different cell cycle processes. In this work, we identified and characterized SmdA as a novel factor essential for cell morphology and cell division in *S. aureus*. Based on the results presented here, future research should aim at pinpointing the molecular mechanism by which SmdA affects different stages of the cell division process. Finally, because SmdA depletion results in increased sensitivity to β-lactams, it may as such also be a possible future target for combatting β-lactam resistance by resensitizing MRSA to these antibiotics.

MATERIALS AND METHODS

Bacterial strains, growth conditions, and transformations. *Escherichia coli* IM08B (64), *E. coli* XL1-Blue, and *E. coli* BTH101 were grown in lysogeny broth (LB) at 30 to 37°C with shaking or on lysogeny agar (LA) plates at 30 to 37°C, with 100 μg/mL ampicillin and/or 50 μg/mL kanamycin for selection. *S. aureus* SH1000, NCTC8325-4, HG001, and COL were grown in brain heart infusion (BHI) broth or tryptic soy broth (TSB) at 37°C with shaking or on BHI plates at 37°C. For selection, 10 μg/mL of chloramphenicol, 5 μg/mL of erythromycin, 15 μg/mL neomycin or 100 μg/mL spectinomycin were added. For induction of gene expression, 50 or 300 μM isopropyl β-D-1-thiogalactopyranoside (IPTG) or 2.5 ng/mL anhydrotetracycline (ATc) were added to the bacterial cultures.

A standard heat shock protocol was used for the transformation of *E. coli* IM08B. Isolated plasmids from *E. coli* were transformed into *S. aureus* by electroporation. Preparation of electrocompetent *S. aureus* cells and electroporation were performed according to Löfblom et al. (65). Bacterial strains used in this study are listed in Table S2.

Genetic modifications. For all cloning, DNA fragments were amplified from *S. aureus* SH1000 genomic DNA, and cloning was performed with restriction digestion (New England Biolabs [NEB]) and subsequent ligation using T4 DNA Ligase (NEB) unless otherwise stated. Ligation mixtures were transformed into *E. coli* IM08B and sequence-verified plasmids were transformed into *S. aureus*. All strains and primers used in this study are listed in Table S2 and Table S3, respectively.

Fluorescent fusion constructs. (i) Construction of pLOW-smdA-*m*(*sf*)*gfp*. Monomeric superfolder GFP, *m*(*sf*)*gfp*, was initially fused to *ftsZ* in the plasmid pLOW (35). *m*(*sf*)*gfp* was amplified from the plasmid pMK17 (66) using forward primer im1_linker_FP_F_BamHI (annealing to the linker sequence) and reverse primer im2_m(sf)gfp_R_NotI_EcoRI. The amplified fragment encodes a linker sequence N-terminally of the *m*(*sf*)*gfp* gene. The fragment was digested with BamHI and EcoRI and subsequently ligated

into the corresponding sites of the plasmid pLOW-*ftsZ-gfp* to replace the original *gfp*-gene with the linker_m(sf)gfp sequence. SAOUSHSC_01908 was then amplified with primers im77_SA1908_F_SalI_RBS and im78_SA1908_R_BamHI, the product was digested with SalI and BamHI and ligated into the corresponding sites of pLOW-*ftsZ-m*(*sf*)*gfp* to create pLOW-*smdA-m*(*sf*)*gfp*.

(ii) Construction of pMAD-smdA-*m*(*sf*)*gfp_aad9* for chromosomal integration. To tag the chromosomal *smdA*, the plasmid pMAD-*smdA-flag_aad9* was constructed initially. The insert in this plasmid (*smdA-flag_aad9*) was assembled by overlap extension PCR (primers im147-im152) with the flag-tag sequence inserted by primer overhangs and cloned into pMAD (34) using restriction enzymes MluI and BamHI and T4 DNA Ligase (NEB). The insert was designed so that the flag-tag could be removed using NotI and SpeI. The *m*(*sf*)*gfp* sequence was amplified from template pMK17 (66) using the primers im153 and im154. The PCR product was digested with NotI and SpeI and subsequently ligated with NotI- and SpeI-digested pMAD-*smdA-flag_aad9*. The ligation mix was transformed to *E. coli* IM08B, and the resulting plasmid, pMAD-*smdA-m*(*sf*)*gfp_aad9*, was verified by sequencing and transformed into electrocompetent *S. aureus* SH1000. Integration of *smdA-m*(*sf*)*gfp* in the native locus of *smdA* using the temperature-sensitive pMAD-system was carried out as previously described (34).

(iii) Construction of pHC-ftsZ-mKate2. *ftsZ-mKate2* was amplified from the plasmid pLOW-*ftsZ-mKate2*. pLOW-*ftsZ-mKate2* was made in a similar manner as described for pLOW-*ftsZ-m*(*sf*)*gfp* but with reverse primer im5_mKate_R_NotI_EcoRI and genomic DNA derived from strain MK119 (67) as the template for amplification of *mKate2*. *ftsZ-mKate2* was then amplified with primers USHC109 and USHC148, generating a product with SalI and MluI as an overhang. The PCR product and the plasmid pSK9065 (68) were digested with SalI and MluI and thereafter ligated.

(iv) Construction of pLOW-smdA-mYFP. This plasmid was constructed by using pLOW-*ftsZ-mYFP* as starting point, made similarly as described for pLOW-*ftsZ-m*(*sf*)*gfp* but with reverse primer im3_cfp_myfp_R_NotI_EcoRI and plasmid pMK20 (lab collection) as the template for amplifying *mYFP*. The plasmids pLOW-*smdA-m*(*sf*)*gfp* (described above) and pLOW-*ftsZ-mYFP* were digested with SalI and BamHI and subsequently ligated, resulting in pLOW-*smdA-mYFP*.

CRISPRi constructs. (i) Construction of pCG248-sgRNA(smdA). For gene knockdowns, the CRISPR interference (CRISPRi) system developed by Stamsås et al. (69) was used. In this system, *dcas9* is placed downstream of an IPTG-inducible promoter in the plasmid pLOW-*dcas9*. A second plasmid is carrying the single guide RNA (pCG248-sgRNA[*x*], where *x* represents the targeted gene), which constitutively expresses the sgRNA, including the 20 nt base-pairing regions specific for the gene to be knocked down. The pLOW-*dcas9* plasmid contains an erythromycin resistance gene and the pCG248-sgRNA(*x*) plasmid is a chloramphenicol resistance gene. The gene-specific 20 nt sequences were replaced in the pCG248-sgRNA(*x*) plasmids using an inverse PCR approach as described earlier (69) using primers mk299 and mk323.

(ii) Construction of pLOW-dCas9_aad9. To make the CRISPRi system compatible with the MRSA strain COL (which is intrinsically erythromycin resistant), the erythromycin resistance gene *ermC* in pLOW-*dcas9* was replaced with *aad9*, encoding a spectinomycin resistance cassette. The primers im183 and im184 were used to amplify the entire pLOW-*dcas9* plasmid, except the *ermC* gene. The *aad9* gene was amplified with primers im185 and im186 using pCN55 (70) as the template, where im185 contained the sequence of im183 as overhang, and im186 the sequence of im184 as an overhang. Thus, the two fragments had overlapping sequences and were fused using NEBuilder HiFi DNA Assembly (NEB). The construct was transformed to *E. coli* IM08B, and the plasmid was verified by PCR and sequencing. For CRISPRi in *S. aureus* COL, the pLOW-*dcas9_aad9* plasmid was used along with pCG248-sgRNA(*x*).

Construction of plasmids used for overexpression studies. (i) Construction of pLOW-smdA and mutated versions. *smdA* was amplified from *S. aureus* genomic DNA using primers im77_SA1908_F_SalI_RBS and mk517_1908_R_NotI. The fragment was digested with SalI and NotI and ligated into the corresponding sites of plasmid pLOW-*dcas9* (69) to produce the plasmid pLOW-*smdA*, with IPTG-inducible overexpression of *smdA*. pLOW-*smdA*Δ*TMH* was constructed in a similar manner, except that primer, mk518_1908_F_RBS_SalI was used instead of im77 to remove the 29 N-terminal amino acids of SmdA, predicted to encode the TMH and extracellular part. Site-directed mutagenesis in the two plasmids was performed by a two-step overlap extension PCR approach, where the mutations were introduced in the primers. The primers mk519 and mk520 were used for introducing mutation H145A (mut1), mut2 (R150A, R151A) was made with primers mk521 and mk522, and mut3 (F280A, H281A) with primers mk529 and mk530.

Phase-contrast and fluorescence microscopy analysis. For induction of plasmid-encoded fluorescent fusions, exponentially growing cultures were diluted to OD_{600} 0.05 in BHI medium with 50 μM IPTG and incubated for 2 h before microscopy. For CRISPRi-knockdown and overexpression experiments, cultures of OD_{600} = 0.4 were diluted 250-fold in medium with 300 μM IPTG and grown until OD_{600} was approximately 0.4. For labeling of the cell wall, BODIPY^{TM} FL vancomycin (VanFL) (Invitrogen) was added. To label newly synthesized peptidoglycan, HADA (van Nieuwenhze group, Indiana University) was added actively growing cultures (OD_{600} approximately 0.4) at a final concentration of 250 μM. The cells were incubated with HADA at 37°C for 90 sec and then put on ice. The cultures were pelleted by centrifugation at 10 000 $\times$ *g* at 4°C for 1 min, washed with cold 1 $\times$ PBS, pH 7.4 and finally resuspended in 25 μL PBS. Cells were subsequently added to agarose pads and microscopy was performed on a Zeiss AxioObserver with ZEN Blue software. An ORCAFlash4.0 V2 Digital complementary metal-oxide-semiconductor (CMOS) camera (Hamamatsu Photonics) was used to capture images through a 100 $\times$ PC objective. HPX 120 Illuminator (Zeiss) was used as a light source for fluorescence microscopy.

All microscopy analyses were repeated at least two times. Images were processed and prepared for publication using Fiji (71). For analysis of cell roundness, cell area, and fluorescent labeling patterns,

MicrobeJ (72) was used to determine cell outlines. Outlines were corrected manually, when necessary. Cell area and roundness as a measure of morphology were calculated and plotted using MicrobeJ. After cell outline detection, categorization of cells into normal or abnormal labeling patterns was done manually using images from independent experiments. The septum/periphery fluorescence signal ratio was measured as described before (73) in cells with a full septal signal of SmdA-GFP. A fluoresce ratio between 2.5 and 3.5 is typical for septum-enriched proteins (11).

Structured illumination microscopy (SIM) and stimulated emission depletion (STED) microscopy. Super-resolution SIM imaging was performed using a Zeiss ELYRA PS.1 microscope equipped with a 100 × 1.46 NA alpha plan apochromat oil immersion objective and a pco.edge sCMOS camera. Fluorescence images were acquired sequentially using 200 to 300 ms exposure times per image, for a total of 15 images per SIM reconstruction. All imaging was performed at room temperature (~23°C). Raw data were reconstructed using the SIM algorithms in ZEN 2011 SP7 software (black edition, Carl Zeiss). Brightfield images were captured using widefield imaging mode. Images had a final pixel size of 25 nm.

Gated STED (gSTED) images were acquired on a Leica TCS SP8 STED 3× system, using an HC PL Apo 100 × oil immersion objective with NA 1.40. Fluorophores were excited using a white excitation laser operated at 509 nm for mYFP and 563 nm for mKate2. A STED depletion laser line was operated at 592 nm and 775 nm for mYFP and mKate2, respectively, using a detection time delay of 0.8 to 1.6 ns for both fluorophores. The total depletion laser intensity was in the order of 20 to 40 MW cm^{-2} for all STED imaging. The final pixel size was 13 nm, and the scanning speed was 400 Hz. The pinhole size was set to 0.9 AU.

Images were processed and analyzed using Fiji (71). Line scans were analyzed using the Plot Profile function in Fiji, using a line width of 1.5. Fluorescence intensities were normalized to the highest value for each channel.

Scanning and transmission electron microscopy analysis. Overnight cultures were diluted to approximately OD_{600} = 0.1 in BHI. When OD_{600} reached 0.4, the cultures were diluted at 1:250. Antibiotics and IPTG were added when appropriate. The cultures (10 mL) were grown to OD_{600} = 0.3 and 1 volume of fixation solution, containing 5% (wt/vol) glutaraldehyde and 4% (wt/vol) paraformaldehyde in 1×PBS, pH 7.4, was added. The tubes were carefully inverted a few times and incubated for 1 h at room temperature before being placed at 4°C overnight. The following day, the cultures were centrifuged at 5000 × *g*, and the pellets were washed three times with PBS. Further preparations of samples to be analyzed with TEM were performed as described before (69).

Samples for SEM were, after washing with PBS, dehydrated with EtOH, essentially in the same manner as for sample preparations for TEM (69). The samples were subjected to critical point drying by exchanging the EtOH with CO_2. The samples were then coated with a conductive layer of Au-Pd before being analyzed in a Zeiss EVO50 EP Scanning electron microscope. Images were analyzed and prepared using Fiji (71).

Growth assays. For examining growth on solid medium, overnight cultures were diluted 1:250 in BHI containing 300 μM IPTG, unless otherwise specified. When reaching the exponential-phase, OD_{600} was adjusted to 0.3 for all samples. A 10-fold dilution series were made for all strains, and 2 μL of each dilution were spotted on BHI agar containing proper antibiotics and 300 μM IPTG. The plates were incubated at 37°C for approximately 16 h, and pictures of the plates were captured in a Gel Doc™ XR + Imager (Bio-Rad).

For measurement of growth in liquid cultures, cells were at OD_{600} 0.4, were diluted 1:250 in a medium containing 300 μM IPTG. Every hour for 5 h, OD_{600} was measured spectrophotometrically using Genesys 30 (Thermo Scientific) and dilutions of the cultures were plated for CFU counting.

MIC assays. The experiments were set up in 96-well microtiter plates with a total volume of 300 μL. A 2-fold dilution series of the antibiotics were prepared in BHI containing selective antibiotics and IPTG when appropriate. The overnight cultures were diluted 1:1000 in BHI containing 300 μg/mL IPTG for induction. The cells were grown at 37°C, and the plate was shaken for 5 sec before measurements of OD_{600} were taken every 10th min throughout the experiment, using either a Synergy™ H1 Hybrid Multi-Mode Reader (BioTek Instruments) or a Hidex Sense (Hidex Oy). The experiments were repeated at least two times with the same results.

RNA isolation and RT-PCR. To verify that *smdA* expression was knocked down by CRISPRi, RNA was isolated from exponentially growing cultures of IM284 (SH1000, CRISPRi[control]), IM165 (SH000 CRISPRi [empty]), and IM269 (SH1000 CRISPRi[*smdA*]). Isolation of total RNA and cDNA synthesis were performed as previously described (69). A PCR (30 cycles) was run with Phusion High-Fidelity DNA polymerase (NEB). The primer pairs im126/im127 and im137/im138 were used to target the reference gene *pta* (74) and *smdA*, respectively.

Detection of lipoteichoic acid (LTA) by Western blotting. Detection of LTA was performed by Western blotting, and sample preparations were done according to descriptions found in Hesser et al. (26). Cells were grown in TSB medium. The samples were separated on a 4 to 20% gradient Mini Protean TGX acrylamide gel (Bio-Rad) and subsequently transferred to a polyvinylidene difluoride (PVDF) membrane by semidry electroblotting. The membrane was blocked for 1 h in 5% (wt/vol) skim milk in PBST and placed overnight at 4°C. Next, the membrane was incubated for 1 h with α-LTA (Hycult) 1:4000 in PBST, washed three times (10 min each) with PBST before incubation for 1 h with α-Mouse IgG HRP Conjugate (Promega) secondary antibody (1:10 000 in PBST). The membrane was again washed three times and LTA bands were visualized by using SuperSignal™ West Pico PLUS Chemiluminescent substrate (Thermo Fisher Scientific) in an Azure Imager c400 (Azure Biosystems).

The same procedure as in (44) was carried out for possible detection of LTA released to the medium. The supernatants, after harvesting cells during sample preparations, were kept. Supernatant samples were centrifuged for 16 000 × *g* for 10 min, and 75 μL was mixed with 25 μL 4× SDS-PAGE sample

buffer. These samples were boiled for 30 min and applied on the 4 to 20% Mini Protean TGX acrylamide gel. Thereafter, the same immunodetection procedure as described above was followed.

Fourier-transform infrared spectroscopy (FTIR) analysis. Cultures of the strains IM313 (HG001, CRISPRi[control]), IM312 (HG001, CRISPRi[*smdA*]) and IM357 (HG001, CRISPRi[*tarO*]) were initially pregrown in BHI to exponential-phase, back diluted to OD_{600} = 0.05 and induced with 300 μM IPTG. The bacterial cells (1 mL) were harvested at OD_{600} = 0.4 by centrifugation at 5000 $\times$ *g*, 4°C, for 3 min. The pelleted cells were kept at −20°C before further processing. Pellets were resuspended in 40 μL 0.1% (wt/vol) NaCl, and 10 μL of the suspensions were added to an IR-light-transparent silicon 384-well microplate (Bruker Optic, Germany), with three technical replicates for each sample. The plates were left to dry at room temperature for approximately 2 h. FTIR spectra were recorded in transmission mode using a high-throughput screening extension (HTS-XT) unit coupled to a Vertex 70 FTIR spectrometer (Bruker Optik GmbH, Leipzig, Germany). Spectra were recorded in the region 4000 to 500 cm^{-1}, with a spectral resolution of 6 cm^{-1}, a digital spacing of 1.928 cm^{-1}, and an aperture of 5 mm. For each spectrum, 64 scans were averaged. The OPUS software (Bruker Optik GmbH, Leipzig, Germany) was used for data acquisition and instrument control. The obtained spectra were processed by taking second derivatives and extended multiplicative signal correction (EMSC) preprocessing in Unscrambler X version 11 (CAMO Analytics, Oslo, Norway). The results presented are averaged spectra from 3 biological replicates (each with 3 technical replicates) for the region with wavelengths between 1200 cm^{-1} and 800 cm^{-1}.

GFP-trap and liquid chromatography with tandem mass spectrometry (LC-MS/MS). Cultures (*S. aureus* SH1000 wild-type, IM308 SH1000 *smdA-m(sf)gfp*, IM104 SH1000 pLOW-*smdA-m(sf)gfp* and IM164 SH1000 pLOW-*smdA-flag*) were pregrown in BHI to exponential-phase, back diluted to OD_{600} = 0.05 and induced if necessary. When reaching OD_{600} at 0.4, 80 mL of each culture was harvested by centrifugation at 4000 $\times$ *g*, 4°C for 3 min. Supernatants were decanted and pellets resuspended in cold TBS before transfer to 1.5 mL microcentrifuge tubes. Centrifugation was repeated for 1 min, and pelleted cells were stored at −80°C before further use.

For GFP-trap, cells were resuspended in 1 mL cold buffer containing 10 mM Tris pH 7.5, 150 mM NaCl, 1 mM PMSF, 6 μg/mL RNase and 6 μg/mL DNase. Suspensions were transferred to 2 mL lysing matrix B tubes (MP Biomedicals) containing 0.8 g $\leq$ 106 μm glass beads (Sigma-Aldrich) and subjected for mechanical lysis by agitation in a FastPrep-24™ (MP Biomedicals) for 3 $\times$ 30 sec at 6.5 m/s, with 1 min pause on ice between the runs. Tubes were centrifuged at 5000 $\times$ *g*, 4°C for 10 min, and supernatants were transferred to new tubes. Concentrations were determined by measuring Abs280 using NanoDrop™ 2000 (Thermo Fisher Scientific), where a small amount of the samples were added to a final concentration of 1% (wt/vol) SDS before measurements. GFP-Trap beads (25 μL per sample) (Chromotek) were washed three times with 500 μL ice-cold Dilution/Wash buffer (10 mM Tris pH 7.5, 150 mM NaCl, 0.5 mM EDTA) and centrifuged at 2500 $\times$ *g*, 4°C for 5 min. Lysates were diluted in Dilution/Wash buffer to a final concentration of 1 mg in a total volume of 500 μL, before being transferred to GFP-Trap beads. Samples were placed in a Bio RS-24 Multi rotor (Biosan) at 4°C for 1 h. The samples were then centrifuged at 2500 $\times$ *g*, 4°C for 5 min, the supernatant removed, and beads washed three times with Dilution/Wash buffer. During the last washing step, solutions were transferred to new tubes, and after centrifugation and removal of the supernatant, beads were resuspended in 50 μL 5% (wt/vol) SDS, 50 mM Tris pH 7.6. Tubes were incubated at 95°C for 5 min and centrifuged at maximum speed for 30 sec. After standing at the bench for a few minutes,30 to 50 μL were transferred into new tubes. Samples were kept at −20°C and heated for 2 min at 95°C before the sample preparation method Suspension trapping (STrap), conducted as described by Zougman et al. (75).

The peptide samples were analyzed by coupling a nano UPLC (nanoElute, Bruker) to a trapped ion mobility spectrometry/quadrupole time of flight mass spectrometer (timsTOF Pro, Bruker). The peptides were separated by an Aurora Series 1.6 μm C18 reverse-phase 25 cm $\times$ 75 μm analytical column with nanoZero and CaptiveSpray Insert (IonOpticks, Australia). The flow rate was set to 400 nL/min and the peptides were separated using a gradient from 2% to 95% acetonitrile solution (in 0.1% [vol/vol] formic acid) over 120 min. The timsTOF Pro was run in positive ion data-dependent acquisition PASEF mode, with a mass range at 100 to 1700 *m/z*. The acquired spectra were analyzed against an *S. aureus* NCTC8325 proteome database.

Bacterial two-hybrid (BACTH) assays. Plasmid construction, and procedure for the BACTH assays, were conducted in the same manner as previously described (69), and primers used are listed in Table S3. Briefly, gene fusions of selected genes, to the T18 or T25 domains of adenylate cyclase form *Bordetella pertussis*, were made by restriction cutting and ligation in the plasmid vectors pKT25, pKNT25, pUT18, or pUT18C (Euromedex). *E. coli* XL1-Blue cells were used for transformation, and plasmids were verified by sequencing before BACTH assays (76) were set up according to the manufacturer (Euromedex). Cotransformation of plasmids containing fusion-genes of opposite domains, that is T25 in one plasmid and T18 in the other were done in *E. coli* BTH101 with 50 μg/mL kanamycin and 100 μg/mL ampicillin as selection markers. Five random colonies were picked, grown in liquid LB to visible growth, and spotted on LA plates containing 40 μg/mL X-gal and 0.5 mM IPTG, in addition to the selection markers. Plates were incubated dark at 30°C for 20 to 48 h before being inspected, and blue colonies are an indication of positive interaction between tested genes. Presented results are representative of at least six independent replicates.

SUPPLEMENTAL MATERIAL

Supplemental material is available online only.

FIG S1, PDF file, 0.2 MB.

FIG S2, PDF file, 0.3 MB.

FIG S3, PDF file, 0.5 MB.
FIG S4, PDF file, 0.4 MB.
FIG S5, PDF file, 0.2 MB.
FIG S6, PDF file, 0.3 MB.
FIG S7, PDF file, 0.1 MB.
TABLE S1, PDF file, 0.2 MB.
TABLE S2, PDF file, 0.3 MB.
TABLE S3, PDF file, 0.2 MB.

ACKNOWLEDGMENTS

We acknowledge the NMBU Imaging Center for help with electron microscopy, Maria Victoria Heggenhougen and Marita Torrissen Mårli (both NMBU) for access to unpublished strains, and Henriette Olsen (NMBU) for help with FTIR. Mass spectrometry-based proteomic analyses were performed by the MS and Proteomics Core Facility, Norwegian University of Life Sciences (NMBU). This facility is a member of the National Network of Advanced Proteomics Infrastructure (NAPI), which is funded by the Research Council of Norway INFRASTRUKTUR-program (project number: 295910). We acknowledge the van Nieuwenhze group, Indiana University, for providing HADA.

The work is supported by grants from the Research Council of Norway (project number 250976) and JPI-AMR (project number 296906). Work in the Structural Cell Biology Unit (OIST) is supported by OIST core subsidy. Ine S. Myrbråten acknowledges support from Pasteurlegatet.

We declare no conflict of interest.

REFERENCES

1. Sass P, Brötz-Oesterhelt H. 2013. Bacterial cell division as a target for new antibiotics. Curr Opin Microbiol 16:522–530. https://doi.org/10.1016/j.mib.2013.07.006.
2. Pinho MG, Kjos M, Veening J-W. 2013. How to get (a) round: mechanisms controlling growth and division of coccoid bacteria. Nat Rev Microbiol 11:601–614. https://doi.org/10.1038/nrmicro3088.
3. Errington J, Daniel RA, Scheffers D-J. 2003. Cytokinesis in bacteria. Microbiol Mol Biol Rev 67:52–65. https://doi.org/10.1128/MMBR.67.1.52-65.2003.
4. Saraiva BM, Sorg M, Pereira AR, Ferreira MJ, Caulat LC, Reichmann NT, Pinho MG. 2020. Reassessment of the distinctive geometry of *Staphylococcus aureus* cell division. Nat Comm 11:4097. https://doi.org/10.1038/s41467-020-17940-9.
5. Veiga H, Jorge AM, Pinho MG. 2011. Absence of nucleoid occlusion effector Noc impairs formation of orthogonal FtsZ rings during *Staphylococcus aureus* cell division. Mol Microbiol 80:1366–1380. https://doi.org/10.1111/j.1365-2958.2011.07651.x.
6. Gallay C, Sanselicio S, Anderson ME, Soh YM, Liu X, Stamsås GA, Pelliciari S, van Raaphorst R, Dénéréaz J, Kjos M, Murray H, Gruber S, Grossman AD, Veening JW. 2021. CcrZ is a pneumococcal spatiotemporal cell cycle regulator that interacts with FtsZ and controls DNA replication by modulating the activity of DnaA. Nat Microbiol 6:1175–1187. https://doi.org/10.1038/s41564-021-00949-1.
7. Barreteau H, Kovač A, Boniface A, Sova M, Gobec S, Blanot D. 2008. Cytoplasmic steps of peptidoglycan biosynthesis. FEMS Microbiol Rev 32:168–207. https://doi.org/10.1111/j.1574-6976.2008.00104.x.
8. Bouhss A, Trunkfield AE, Bugg TD, Mengin-Lecreulx D. 2008. The biosynthesis of peptidoglycan lipid-linked intermediates. FEMS Microbiol Rev 32:208–233. https://doi.org/10.1111/j.1574-6976.2007.00089.x.
9. Rohrer S, Berger-Bächi B. 2003. FemABX peptidyl transferases: a link between branched-chain cell wall peptide formation and β-lactam resistance in gram-positive cocci. Antimicrob Agents Chemother 47:837–846. https://doi.org/10.1128/AAC.47.3.837-846.2003.
10. Sham L-T, Butler EK, Lebar MD, Kahne D, Bernhardt TG, Ruiz N. 2014. Bacterial cell wall. MurJ is the flippase of lipid-linked precursors for peptidoglycan biogenesis. Science 345:220–222. https://doi.org/10.1126/science.1254522.
11. Monteiro JM, Pereira AR, Reichmann NT, Saraiva BM, Fernandes PB, Veiga H, Tavares AC, Santos M, Ferreira MT, Macario V, VanNieuwenhze MS, Filipe SR, Pinho MG. 2018. Peptidoglycan synthesis drives an FtsZ-treadmilling-independent step of cytokinesis. Nature 554:528–532. https://doi.org/10.1038/nature25506.
12. Reichmann NT, Tavares AC, Saraiva BM, Jousselin A, Reed P, Pereira AR, Monteiro JM, Sobral RG, VanNieuwenhze MS, Fernandes F, Pinho MG. 2019. SEDS-bPBP pairs direct lateral and septal peptidoglycan synthesis in *Staphylococcus aureus*. Nat Microbiol 4:1368–1377. https://doi.org/10.1038/s41564-019-0437-2.
13. Meeske AJ, Riley EP, Robins WP, Uehara T, Mekalanos JJ, Kahne D, Walker S, Kruse AC, Bernhardt TG, Rudner DZ. 2016. SEDS proteins are a widespread family of bacterial cell wall polymerases. Nature 537:634–638. https://doi.org/10.1038/nature19331.
14. Wyke AW, Ward JB, Hayes MV, Curtis NA. 1981. A role *in vivo* for penicillin-binding protein-4 of *Staphylococcus aureus*. Eur J Biochem 119:389–393. https://doi.org/10.1111/j.1432-1033.1981.tb05620.x.
15. Atilano ML, Pereira PM, Yates J, Reed P, Veiga H, Pinho MG, Filipe SR. 2010. Teichoic acids are temporal and spatial regulators of peptidoglycan cross-linking in *Staphylococcus aureus*. Proc Natl Acad Sci U S A 107:18991–18996. https://doi.org/10.1073/pnas.1004304107.
16. Pinho MG, Errington J. 2005. Recruitment of penicillin-binding protein PBP2 to the division site of *Staphylococcus aureus* is dependent on its transpeptidation substrates. Mol Microbiol 55:799–807. https://doi.org/10.1111/j.1365-2958.2004.04420.x.
17. Hartman BJ, Tomasz A. 1984. Low-affinity penicillin-binding protein associated with beta-lactam resistance in *Staphylococcus aureus*. J Bacteriol 158:513–516. https://doi.org/10.1128/jb.158.2.513-516.1984.
18. Ubukata K, Yamashita N, Konno M. 1985. Occurrence of a beta-lactam-inducible penicillin-binding protein in methicillin-resistant staphylococci. Antimicrob Agents Chemother 27:851–857. https://doi.org/10.1128/AAC.27.5.851.
19. Oshida T, Sugai M, Komatsuzawa H, Hong Y-M, Suginaka H, Tomasz A. 1995. A *Staphylococcus aureus* autolysin that has an N-acetylmuramoyl-L-alanine amidase domain and an endo-beta-N-acetylglucosaminidase domain: cloning, sequence analysis, and characterization. Proc Natl Acad Sci U S A 92:285–289. https://doi.org/10.1073/pnas.92.1.285.
20. Nega M, Tribelli PM, Hipp K, Stahl M, Götz F. 2020. New insights in the coordinated amidase and glucosaminidase activity of the major autolysin (Atl) in *Staphylococcus aureus*. Commun Biol 3:1–10. https://doi.org/10.1038/s42003-020-01405-2.

21. Thalsø-Madsen I, Torrubia FR, Xu L, Petersen A, Jensen C, Frees D. 2019. The Sle1 cell wall amidase is essential for β-lactam resistance in community-acquired methicillin-resistant *Staphylococcus aureus* USA300. Antimicrob Agents Chemother 64:e01931-19. https://doi.org/10.1128/AAC.01931-19.
22. Dubrac S, Boneca IG, Poupel O, Msadek T. 2007. New insights into the WalK/WalR (YycG/YycF) essential signal transduction pathway reveal a major role in controlling cell wall metabolism and biofilm formation in *Staphylococcus aureus*. J Bacteriol 189:8257–8269. https://doi.org/10.1128/JB.00645-07.
23. Zhou X, Halladin DK, Rojas ER, Koslover EF, Lee TK, Huang KC, Theriot JA. 2015. Mechanical crack propagation drives millisecond daughter cell separation in *Staphylococcus aureus*. Science 348:574–578. https://doi.org/10.1126/science.aaa1511.
24. Monteiro JM, Fernandes PB, Vaz F, Pereira AR, Tavares AC, Ferreira MT, Pereira PM, Veiga H, Kuru E, VanNieuwenhze MS. 2015. Cell shape dynamics during the staphylococcal cell cycle. Nat Comm 6:8055. https://doi.org/10.1038/ncomms9055.
25. Brown S, Santa Maria JP, Jr., Walker S. 2013. Wall teichoic acids of Gram-positive bacteria. Annu Rev Microbiol 67:313–336. https://doi.org/10.1146/annurev-micro-092412-155620.
26. Hesser AR, Matano LM, Vickery CR, Wood BM, Santiago AG, Morris HG, Do T, Losick R, Walker S. 2020. The length of lipoteichoic acid polymers controls *Staphylococcus aureus* cell size and envelope integrity. J Bacteriol 202:e00149-20. https://doi.org/10.1128/JB.00149-20.
27. Silber N, Pan S, Schäkermann S, Mayer C, Brötz-Oesterhelt H, Sass P. 2020. Cell division protein FtsZ is unfolded for N-terminal degradation by antibiotic-activated ClpP. mBio 11:e01006-20. https://doi.org/10.1128/mBio.01006-20.
28. Feng J, Michalik S, Varming AN, Andersen JH, Albrecht D, Jelsbak L, Krieger S, Ohlsen K, Hecker M, Gerth U, Ingmer H, Frees D. 2013. Trapping and proteomic identification of cellular substrates of the ClpP protease in *Staphylococcus aureus*. J Proteome Res 12:547–558. https://doi.org/10.1021/pr300394r.
29. Jensen C, Bæk KT, Gallay C, Thalsø-Madsen I, Xu L, Jousselin A, Ruiz Torrubia F, Paulander W, Pereira AR, Veening J-W, Pinho MG, Frees D. 2019. The ClpX chaperone controls autolytic splitting of *Staphylococcus aureus* daughter cells, but is bypassed by β-lactam antibiotics or inhibitors of WTA biosynthesis. PLoS Pathog 15:e1008044. https://doi.org/10.1371/journal.ppat.1008044.
30. Chaudhuri RR, Allen AG, Owen PJ, Shalom G, Stone K, Harrison M, Burgis TA, Lockyer M, Garcia-Lara J, Foster SJ, Pleasance SJ, Peters SE, Maskell DJ, Charles IG. 2009. Comprehensive identification of essential *Staphylococcus aureus* genes using transposon-mediated differential hybridisation (TMDH). BMC Genomics 10:291. https://doi.org/10.1186/1471-2164-10-291.
31. Santiago M, Matano LM, Moussa SH, Gilmore MS, Walker S, Meredith TC. 2015. A new platform for ultra-high density *Staphylococcus aureus* transposon libraries. BMC Genomics 16:1–18. https://doi.org/10.1186/s12864-015-1361-3.
32. Valentino MD, Foulston L, Sadaka A, Kos VN, Villet RA, Santa Maria J, Lazinski DW, Camilli A, Walker S, Hooper DC, Gilmore MS. 2014. Genes contributing to *Staphylococcus aureus* fitness in abscess-and infection-related ecologies. mBio 5:e01729-14–e01714. https://doi.org/10.1128/mBio.01729-14.
33. Grynberg M, Godzik A. 2004. NERD: a DNA processing-related domain present in the anthrax virulence plasmid, pXO1. Trends Biochem Sci 29:106–110. https://doi.org/10.1016/j.tibs.2004.01.002.
34. Arnaud M, Chastanet A, Débarbouillé M. 2004. New vector for efficient allelic replacement in naturally nontransformable, low-GC-content, Gram-positive bacteria. Appl Environ Microbiol 70:6887–6891. https://doi.org/10.1128/AEM.70.11.6887-6891.2004.
35. Liew AT, Theis T, Jensen SO, Garcia-Lara J, Foster SJ, Firth N, Lewis PJ, Harry EJ. 2011. A simple plasmid-based system that allows rapid generation of tightly controlled gene expression in *Staphylococcus aureus*. Microbiology (Reading) 157:666–676. https://doi.org/10.1099/mic.0.045146-0.
36. Reynolds PE. 1989. Structure, biochemistry and mechanism of action of glycopeptide antibiotics. Eur J Clin Microbiol Infect Dis 8:943–950. https://doi.org/10.1007/BF01967563.
37. Campbell J, Singh AK, Santa Maria JP, Jr., Kim Y, Brown S, Swoboda JG, Mylonakis E, Wilkinson BJ, Walker S. 2011. Synthetic lethal compound combinations reveal a fundamental connection between wall teichoic acid and peptidoglycan biosyntheses in *Staphylococcus aureus*. ACS Chem Biol 6:106–116. https://doi.org/10.1021/cb100269f.
38. Campbell J, Singh AK, Swoboda JG, Gilmore MS, Wilkinson BJ, Walker S. 2012. An antibiotic that inhibits a late step in wall teichoic acid biosynthesis induces the cell wall stress stimulon in *Staphylococcus aureus*. Antimicrob Agents Chemother 56:1810–1820. https://doi.org/10.1128/AAC.05938-11.
39. Vickery CR, Wood BM, Morris HG, Losick R, Walker S. 2018. Reconstitution of *Staphylococcus aureus* lipoteichoic acid synthase activity identifies Congo red as a selective inhibitor. J Am Chem Soc 140:876–879. https://doi.org/10.1021/jacs.7b11704.
40. Price NP, Tsvetanova B. 2007. Biosynthesis of the tunicamycins: a review. J Antibiot (Tokyo) 60:485–491. https://doi.org/10.1038/ja.2007.62.
41. Swoboda JG, Campbell J, Meredith TC, Walker S. 2010. Wall teichoic acid function, biosynthesis, and inhibition. Chembiochem 11:35–45. https://doi.org/10.1002/cbic.200900557.
42. Santa Maria JP, Jr., Sadaka A, Moussa SH, Brown S, Zhang YJ, Rubin EJ, Gilmore MS, Walker S. 2014. Compound-gene interaction mapping reveals distinct roles for *Staphylococcus aureus* teichoic acids. Proc Natl Acad Sci U S A 111:12510–12515. https://doi.org/10.1073/pnas.1404099111.
43. Oku Y, Kurokawa K, Matsuo M, Yamada S, Lee B-L, Sekimizu K. 2009. Pleiotropic roles of polyglycerolphosphate synthase of lipoteichoic acid in growth of *Staphylococcus aureus* cells. J Bacteriol 191:141–151. https://doi.org/10.1128/JB.01221-08.
44. Mikkelsen K, Sirisarn W, Alharbi O, Alharbi M, Liu H, Nøhr-Meldgaard K, Mayer K, Vestergaard M, Gallagher LA, Derrick JP, McBain AJ, Biboy J, Vollmer W, O'Gara JP, Grunert T, Ingmer H, Xia G. 2021. The novel membrane-associated auxiliary factors AuxA and AuxB modulate β-lactam resistance in MRSA by stabilizing lipoteichoic acids. Int J Antimicrob Agents 57:106283. https://doi.org/10.1016/j.ijantimicag.2021.106283.
45. Suzuki T, Campbell J, Kim Y, Swoboda JG, Mylonakis E, Walker S, Gilmore MS. 2012. Wall teichoic acid protects *Staphylococcus aureus* from inhibition by Congo red and other dyes. J Antimicrob Chemother 67:2143–2151. https://doi.org/10.1093/jac/dks184.
46. Chan YG-Y, Kim HK, Schneewind O, Missiakas D. 2014. The capsular polysaccharide of *Staphylococcus aureus* is attached to peptidoglycan by the LytR-CpsA-Psr (LCP) family of enzymes. J Biol Chem 289:15680–15690. https://doi.org/10.1074/jbc.M114.567669.
47. Grunert T, Jovanovic D, Sirisarn W, Johler S, Weidenmaier C, Ehling-Schulz M, Xia G. 2018. Analysis of *Staphylococcus aureus* wall teichoic acid glycoepitopes by Fourier Transform Infrared Spectroscopy provides novel insights into the staphylococcal glycocode. Sci Rep 8:9. https://doi.org/10.1038/s41598-018-20222-6.
48. Radkov AD, Hsu Y-P, Booher G, VanNieuwenhze MS. 2018. Imaging bacterial cell wall biosynthesis. Annu Rev Biochem 87:991–1014. https://doi.org/10.1146/annurev-biochem-062917-012921.
49. Biswas R, Voggu L, Simon UK, Hentschel P, Thumm G, Götz F. 2006. Activity of the major staphylococcal autolysin Atl. FEMS Microbiol Lett 259:260–268. https://doi.org/10.1111/j.1574-6968.2006.00281.x.
50. Jorge AM, Hoiczyk E, Gomes JP, Pinho MG. 2011. EzrA contributes to the regulation of cell size in *Staphylococcus aureus*. PLoS One 6:e27542. https://doi.org/10.1371/journal.pone.0027542.
51. Lund VA, Wacnik K, Turner RD, Cotterell BE, Walther CG, Fenn SJ, Grein F, Wollman AJ, Leake MC, Olivier N, Cadby A, Mesnage S, Jones S, Foster SJ. 2018. Molecular coordination of *Staphylococcus aureus* cell division. Elife 7:e32057. https://doi.org/10.7554/eLife.32057.
52. Jumper J, Evans R, Pritzel A, Green T, Figurnov M, Ronneberger O, Tunyasuvunakool K, Bates R, Žídek A, Potapenko A, Bridgland A, Meyer C, Kohl SAA, Ballard AJ, Cowie A, Romera-Paredes B, Nikolov S, Jain R, Adler J, Back T, Petersen S, Reiman D, Clancy E, Zielinski M, Steinegger M, Pacholska M, Berghammer T, Bodenstein S, Silver D, Vinyals O, Senior AW, Kavukcuoglu K, Kohli P, Hassabis D. 2021. Highly accurate protein structure prediction with AlphaFold. Nature 596:583–589. https://doi.org/10.1038/s41586-021-03819-2.
53. Roemer T, Schneider T, Pinho MG. 2013. Auxiliary factors: a chink in the armor of MRSA resistance to β-lactam antibiotics. Curr Opin Microbiol 16:538–548. https://doi.org/10.1016/j.mib.2013.06.012.
54. Tan CM, Therien AG, Lu J, Lee SH, Caron A, Gill CJ, Lebeau-Jacob C, Benton-Perdomo L, Monteiro JM, Pereira PM, Elsen NL, Wu J, Deschamps K, Petcu M, Wong S, Daigneault E, Kramer S, Liang L, Maxwell E, Claveau D, Vaillancourt J, Skorey K, Tam J, Wang H, Meredith TC, Sillaots S, Wang-Jarantow L, Ramtohul Y, Langlois E, Landry F, Reid JC, Parthasarathy G, Sharma S, Baryshnikova A, Lumb KJ, Pinho MG, Soisson SM, Roemer T. 2012. Restoring methicillin-resistant *Staphylococcus aureus* susceptibility to β-lactam antibiotics. Sci Transl Med 4:126ra35. https://doi.org/10.1126/scitranslmed.3003592.
55. Lee SH, Jarantow LW, Wang H, Sillaots S, Cheng H, Meredith TC, Thompson J, Roemer T. 2011. Antagonism of chemical genetic interaction

networks resensitize MRSA to β-lactam antibiotics. Chem Biol 18:1379–1389. https://doi.org/10.1016/j.chembiol.2011.08.015.
56. Brown S, Xia G, Luhachack LG, Campbell J, Meredith TC, Chen C, Winstel V, Gekeler C, Irazoqui JE, Peschel A, Walker S. 2012. Methicillin resistance in *Staphylococcus aureus* requires glycosylated wall teichoic acids. Proc Natl Acad Sci U S A 109:18909–18914. https://doi.org/10.1073/pnas.1209126109.
57. Quiblier C, Zinkernagel AS, Schuepbach RA, Berger-Bächi B, Senn MM. 2011. Contribution of SecDF to *Staphylococcus aureus* resistance and expression of virulence factors. BMC Microbiol 11:72. https://doi.org/10.1186/1471-2180-11-72.
58. Roch M, Lelong E, Panasenko OO, Sierra R, Renzoni A, Kelley WL. 2019. Thermosensitive PBP2a requires extracellular folding factors PrsA and HtrA1 for *Staphylococcus aureus* MRSA β-lactam resistance. Commun Biol 2:417. https://doi.org/10.1038/s42003-019-0667-0.
59. Pereira AR, Hsin J, Król E, Tavares AC, Flores P, Hoiczyk E, Ng N, Dajkovic A, Brun YV, VanNieuwenhze MS, Roemer T, Carballido-Lopez R, Scheffers DJ, Huang KC, Pinho MG. 2016. FtsZ-dependent elongation of a coccoid bacterium. mBio 7:e00908-16. https://doi.org/10.1128/mBio.00908-16.
60. Steele VR, Bottomley AL, Garcia-Lara J, Kasturiarachchi J, Foster SJ. 2011. Multiple essential roles for EzrA in cell division of *Staphylococcus aureus*. Mol Microbiol 80:542–555. https://doi.org/10.1111/j.1365-2958.2011.07591.x.
61. Steczkiewicz K, Muszewska A, Knizewski L, Rychlewski L, Ginalski K. 2012. Sequence, structure and functional diversity of PD-(D/E)XK phosphodiesterase superfamily. Nucleic Acids Res 40:7016–7045. https://doi.org/10.1093/nar/gks382.
62. Kwon A, Scott S, Taujale R, Yeung W, Kochut KJ, Eyers PA, Kannan N. 2019. Tracing the origin and evolution of pseudokinases across the tree of life. Sci Signal 12:eaav3810. https://doi.org/10.1126/scisignal.aav3810.
63. Herbert S, Ziebandt AK, Ohlsen K, Schafer T, Hecker M, Albrecht D, Novick R, Gotz F. 2010. Repair of global regulators in *Staphylococcus aureus* 8325 and comparative analysis with other clinical isolates. Infect Immun 78:2877–2889. https://doi.org/10.1128/IAI.00088-10.
64. Monk IR, Tree JJ, Howden BP, Stinear TP, Foster TJ. 2015. Complete bypass of restriction systems for major *Staphylococcus aureus* lineages. mBio 6:e00308-15–e00315. https://doi.org/10.1128/mBio.00308-15.
65. Löfblom J, Kronqvist N, Uhlén M, Ståhl S, Wernérus H. 2007. Optimization of electroporation-mediated transformation: *Staphylococcus carnosus* as model organism. J Appl Microbiol 102:736–747. https://doi.org/10.1111/j.1365-2672.2006.03127.x.
66. van Raaphorst R, Kjos M, Veening J-W. 2017. Chromosome segregation drives division site selection in *Streptococcus pneumoniae*. Proc Natl Acad Sci U S A 114:E5959–E5968. https://doi.org/10.1073/pnas.1620608114.
67. Kjos M, Veening JW. 2014. Tracking of chromosome dynamics in live *Streptococcus pneumoniae* reveals that transcription promotes chromosome segregation. Mol Microbiol 91:1088–1105. https://doi.org/10.1111/mmi.12517.
68. Brzoska AJ, Firth N. 2013. Two-plasmid vector system for independently controlled expression of green and red fluorescent fusion proteins in *Staphylococcus aureus*. Appl Environ Microbiol 79:3133–3136. https://doi.org/10.1128/AEM.00144-13.
69. Stamsås GA, Myrbråten IS, Straume D, Salehian Z, Veening JW, Håvarstein LS, Kjos M. 2018. CozEa and CozEb play overlapping and essential roles in controlling cell division in *Staphylococcus aureus*. Mol Microbiol 109:615–632. https://doi.org/10.1111/mmi.13999.
70. Charpentier E, Anton AI, Barry P, Alfonso B, Fang Y, Novick RP. 2004. Novel cassette-based shuttle vector system for Gram-positive bacteria. Appl Environ Microbiol 70:6076–6085. https://doi.org/10.1128/AEM.70.10.6076-6085.2004.
71. Schindelin J, Arganda-Carreras I, Frise E, Kaynig V, Longair M, Pietzsch T, Preibisch S, Rueden C, Saalfeld S, Schmid B, Tinevez J-Y, White DJ, Hartenstein V, Eliceiri K, Tomancak P, Cardona A. 2012. Fiji: an open-source platform for biological-image analysis. Nat Methods 9:676–682. https://doi.org/10.1038/nmeth.2019.
72. Ducret A, Quardokus EM, Brun YV. 2016. MicrobeJ, a tool for high throughput bacterial cell detection and quantitative analysis. Nat Microbiol 1:16077. https://doi.org/10.1038/nmicrobiol.2016.77.
73. Pereira PM, Filipe SR, Tomasz A, Pinho MG. 2007. Fluorescence ratio imaging microscopy shows decreased access of vancomycin to cell wall synthetic sites in vancomycin-resistant Staphylococcus aureus. Antimicrob Agents Chemother 51:3627–3633. https://doi.org/10.1128/AAC.00431-07.
74. Valihrach L, Demnerova K. 2012. Impact of normalization method on experimental outcome using RT-qPCR in *Staphylococcus aureus*. J Microbiol Methods 90:214–216. https://doi.org/10.1016/j.mimet.2012.05.008.
75. Zougman A, Selby PJ, Banks RE. 2014. Suspension trapping (STrap) sample preparation method for bottom-up proteomics analysis. Proteomics 14:1006–1000. https://doi.org/10.1002/pmic.201300553.
76. Karimova G, Pidoux J, Ullmann A, Ladant D. 1998. A bacterial two-hybrid system based on a reconstituted signal transduction pathway. Proc Natl Acad Sci U S A 95:5752–5756. https://doi.org/10.1073/pnas.95.10.5752.
77. Omasits U, Ahrens CH, Müller S, Wollscheid B. 2014. Protter: interactive protein feature visualization and integration with experimental proteomic data. Bioinformatics 30:884–886. https://doi.org/10.1093/bioinformatics/btt607.
78. Sievers F, Wilm A, Dineen D, Gibson TJ, Karplus K, Li W, Lopez R, McWilliam H, Remmert M, Söding J, Thompson JD, Higgins DG. 2011. Fast, scalable generation of high-quality protein multiple sequence alignments using Clustal Omega. Mol Syst Biol 7:539. https://doi.org/10.1038/msb.2011.75.